

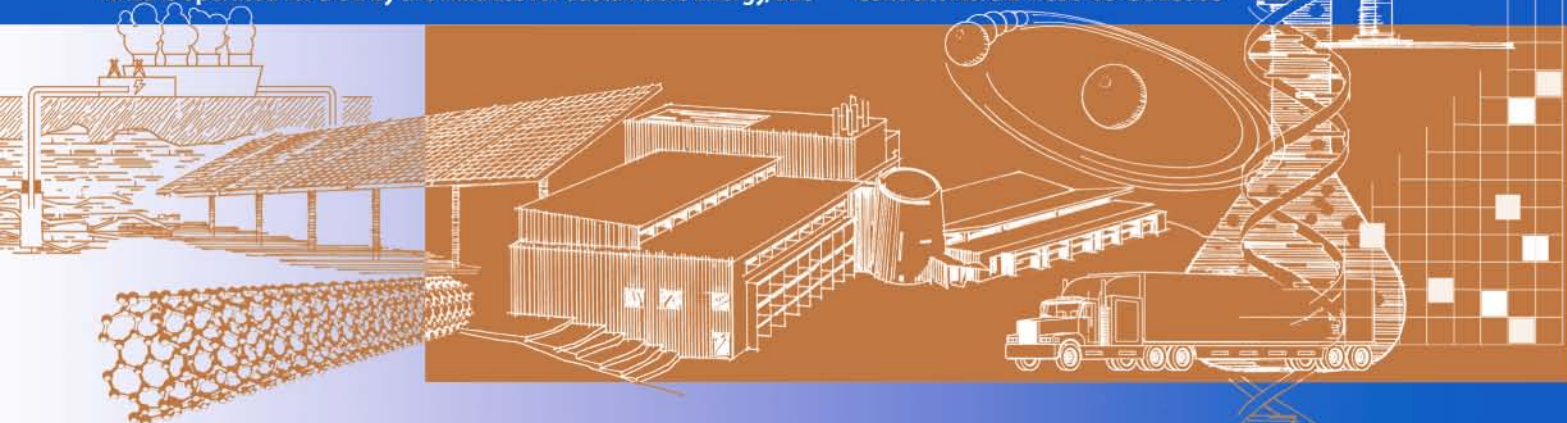
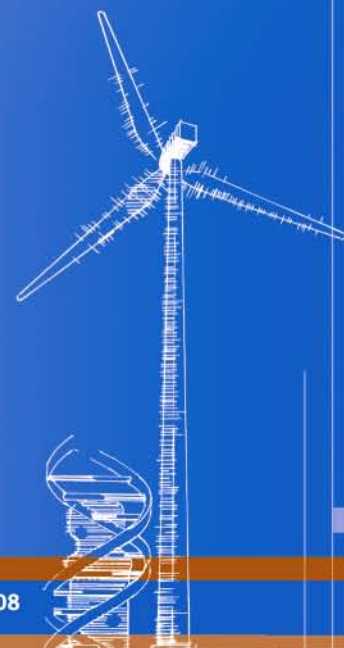


Development of Regional Wind Resource and Wind Plant Output Datasets for the Hawaiian Islands

Final Report

John Manobianco, Charles Alonge, Jaclyn Frank,
and Michael Brower
AWS Truepower, LLC
Albany, New York

Subcontract Report
NREL/SR-550-48680
July 2010



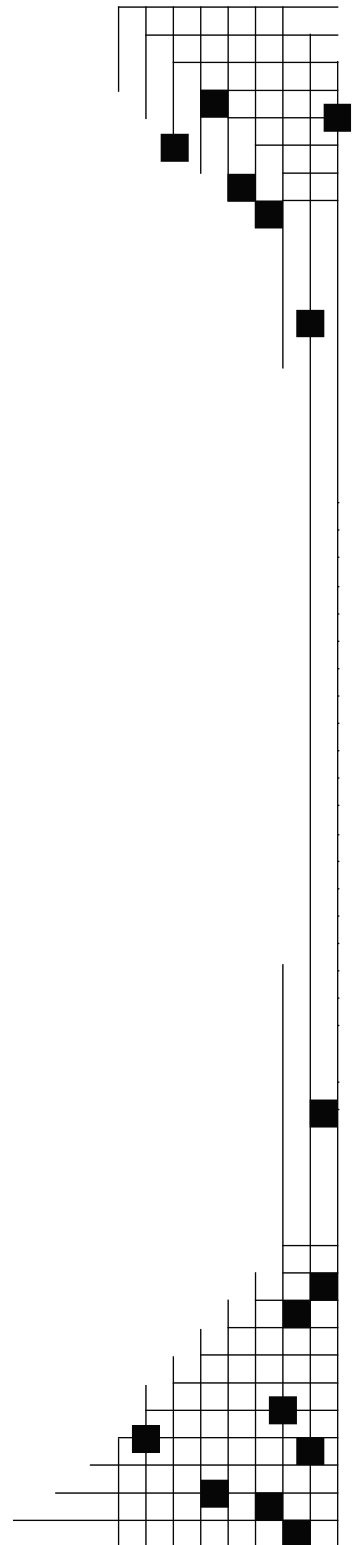
Development of Regional Wind Resource and Wind Plant Output Datasets for the Hawaiian Islands

Final Report

John Manobianco, Charles Alonge, Jaclyn Frank,
and Michael Brower
AWS Truepower, LLC
Albany, New York

NREL Technical Monitor: Debra Lew
Prepared under Subcontract No. ACO-8-88500-01

Subcontract Report
NREL/SR-550-48680
July 2010



National Renewable Energy Laboratory
1617 Cole Boulevard, Golden, Colorado 80401-3393
303-275-3000 • www.nrel.gov

NREL is a national laboratory of the U.S. Department of Energy
Office of Energy Efficiency and Renewable Energy
Operated by the Alliance for Sustainable Energy, LLC

Contract No. DE-AC36-08-GO28308

NOTICE

This report was prepared as an account of work sponsored by an agency of the United States government. Neither the United States government nor any agency thereof, nor any of their employees, makes any warranty, express or implied, or assumes any legal liability or responsibility for the accuracy, completeness, or usefulness of any information, apparatus, product, or process disclosed, or represents that its use would not infringe privately owned rights. Reference herein to any specific commercial product, process, or service by trade name, trademark, manufacturer, or otherwise does not necessarily constitute or imply its endorsement, recommendation, or favoring by the United States government or any agency thereof. The views and opinions of authors expressed herein do not necessarily state or reflect those of the United States government or any agency thereof.

Available electronically at <http://www.osti.gov/bridge>

Available for a processing fee to U.S. Department of Energy and its contractors, in paper, from:

U.S. Department of Energy
Office of Scientific and Technical Information
P.O. Box 62
Oak Ridge, TN 37831-0062
phone: 865.576.8401
fax: 865.576.5728
email: <mailto:reports@adonis.osti.gov>

Available for sale to the public, in paper, from:

U.S. Department of Commerce
National Technical Information Service
5285 Port Royal Road
Springfield, VA 22161
phone: 800.553.6847
fax: 703.605.6900
email: orders@ntis.fedworld.gov
online ordering: <http://www.ntis.gov/ordering.htm>

This publication received minimal editorial review at NREL



Printed on paper containing at least 50% wastepaper, including 20% postconsumer waste

Table of Contents

1	Introduction.....	1
2	Develop Wind Resource Datasets Based on Mesoscale Modeling	2
3	Generate Wind Plant Output.....	4
3.1	Conversion Procedure.....	4
3.2	Validation	8
3.3	Impacts of Model Restart/Assimilation.....	13
4	Forecasts	15
4.1	Forecast Synthesis Procedure	15
4.2	Validation	16
5	High-Frequency Output	19
6	Dataset Usage.....	22
7	Accuracy Summary.....	23
8	Recommendations for Future Work.....	23
9	Conclusions.....	23
10	Acknowledgments.....	23
	APPENDIX.....	24

All figures in this report are attributed to AWS Truepower.

Development of Regional Wind Resource and Wind Plant Output Datasets for the Hawaiian Islands

1 Introduction

In March 2009, AWS Truepower was engaged by the National Renewable Energy Laboratory (NREL) to develop a set of wind resource and plant output data for the Hawaiian Islands. The objective of this project was to expand the methods and techniques employed in the Eastern Wind Integration and Transmission Study (EWITS) to include the state of Hawaii (Figure 1.1). While the Oahu Wind Integration and Transmission Study (OWITS) includes projects in Oahu, Lanai, and Molokai, it was decided that all of Hawaii should be modeled so data would be available for future studies. To support this study, NREL required a set of data that would capture in a realistic fashion both the temporal and spatial variability of the wind resource, and associated wind power generation of onshore projects. These data were to be based on high-resolution simulations of the historical climate performed by a mesoscale numerical weather prediction (NWP) model covering 2007 to 2008.



Figure 1.1 – Hawaiian Islands study region.

AWS Truepower performed this work over a period of six months from March 2009 to August 2009. The work was divided into the following technical tasks:

- Develop wind resource datasets based on mesoscale modeling;
- Generate wind plant output;
- Simulate forecasts;
- Simulate one-minute and two-second samples of wind generation.

This document presents AWS Truepower’s final technical report on the methods used and results achieved for each task. Additional validation results are provided in an appendix.

2 Developing Wind Resource Datasets Based on Mesoscale Modeling

The mesoscale model runs were carried out over a three-month period from March to May, 2009, using the Mesoscale Atmospheric Simulation System (MASS), a proprietary model developed by AWS Truepower partner MESO, Inc. The simulations covered the period 1 January, 2007 to 1 January, 2009 over the Hawaiian Island chain. Table 2.1 summarizes the run configuration.

Table 2.1 – Model configuration for main runs.

Model	MASS v. 6.8
Initialization data source	NCEP/NCAR Global Reanalysis (NNGR; ~1.9° resolution)
Data to be assimilated in the course of simulations (30-, 12-, and 4-km grids only)	Rawinsonde, METAR surface observations (temperature, dew point, wind direction and speed, pressure)
Sea-surface temperatures	MODIS (1-km satellite-based)
High-resolution terrain and land cover (1-km grid only)	USGS 30-m NED and 90-m NLCD
Cumulus scheme (30- and 12-km grids only)	Kain-Fritsch
Spin-up	12 hours before start of valid run
Length of run	15- to 16-day series (e.g., 1–15 Jan, 16–31 Jan)
Frequency of data sampling	10 minutes
Data to be stored	U, V, temperature, pressure, turbulent kinetic energy (TKE) at five heights; surface temperature and pressure, specific humidity, incoming long-wave and short-wave radiation, precipitation

The runs employed a nested grid scheme with horizontal resolutions of 30 km, 12 km, 4 km, and 1 km. The grid layout is shown in Figure 2.1. Figure 2.2 shows the inner 4-km and 1-km grids, along with the locations of rawinsonde data (black stars) and METAR surface observations (red circles) assimilated in the model. Blue triangles note the locations of existing plants. Additionally, locations of stations with long-term records used to compare the strength of the wind resource between 2007 and 2008 (as discussed in Section 3.2) are shown by green pentagons.

Data extraction was carried out for all grid points associated with a project site. For each grid point, four files were produced: (i) surface pressure, (ii) 2-m temperature, (iii) 60-m speed, direction, air density, and turbulent kinetic energy (TKE), and (iv) 80-m speed, direction, air density, and TKE. Each file contains 105,407 records spanning 2007 and 2008 (a leap year) in 10-minute increments. The naming convention is as follows: GRID_XX_IIIJJ_HHHH.TXT, where XX refers to the grid number (from one to four), III and JJJ to the grid point column and row numbers, and HHHH to the height (0000M = surface pressure, 0002M = 2-m temperature, 0060M = 60-m speed, and 0080M = 80-m speed). An example 80-m file is provided in Table 3.2. These files were generated for each grid point within each proposed site. Ten-minute model output at 10, 50, 80, 100, and 200 m above ground level for each grid point were delivered to NREL at a later date.

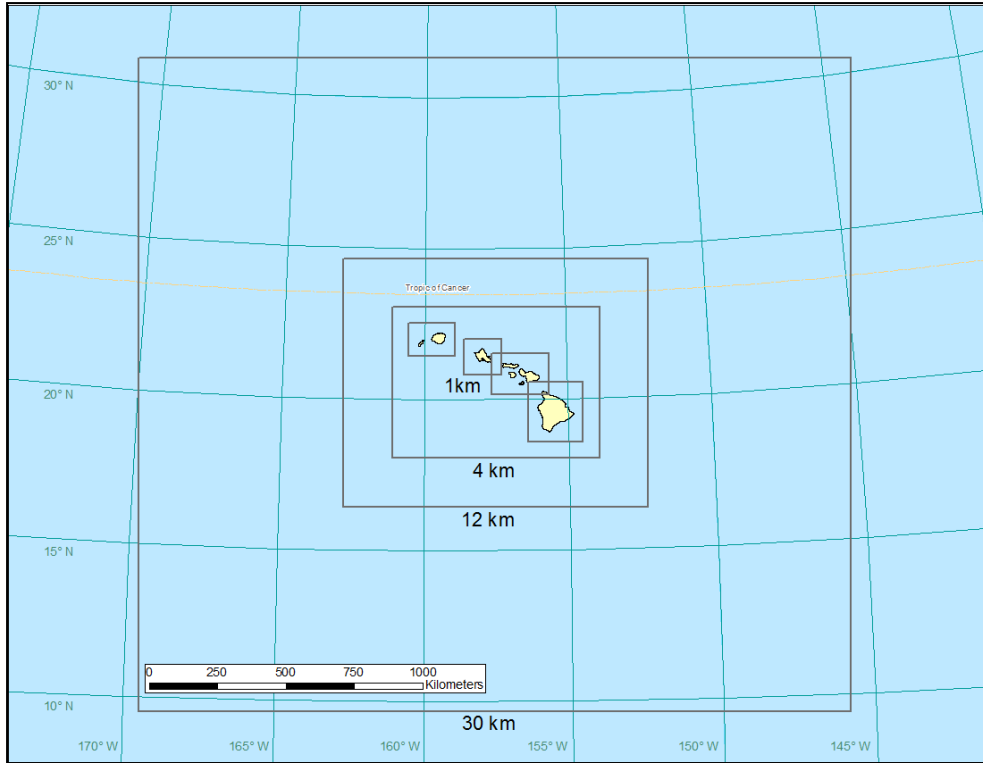


Figure 2.1 – MASS grid definitions.

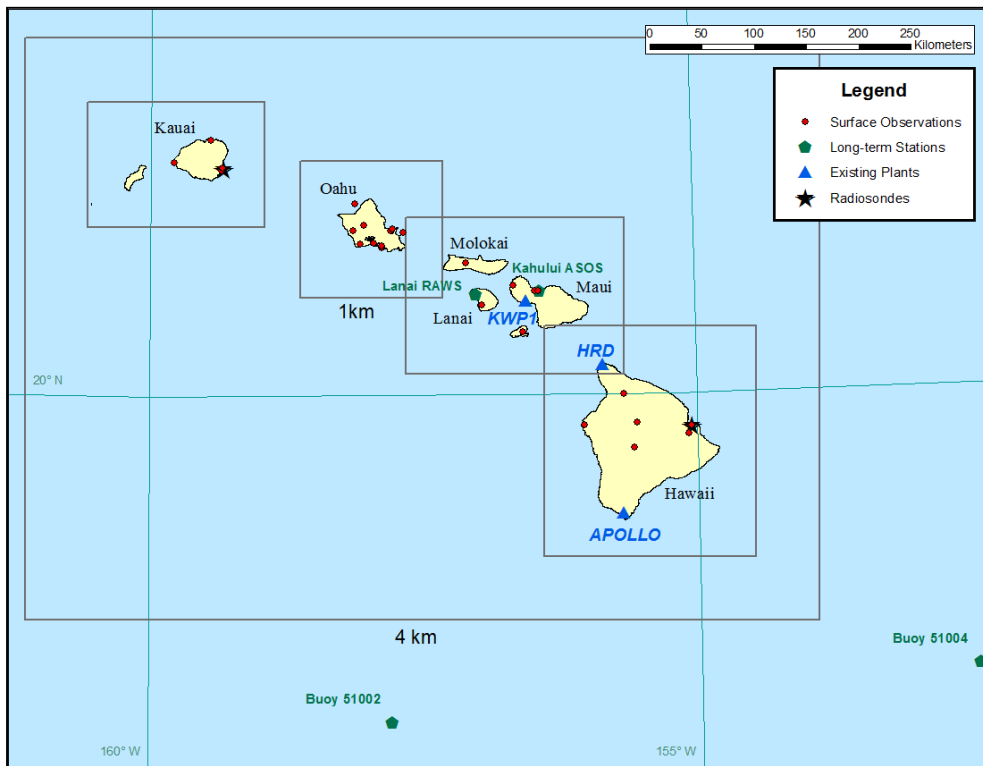


Figure 2.2 – Inner 4- and 1-km MASS grids, along with locations of rawinsondes (black stars) and METAR surface observations (red circles) assimilated into the model. Existing plants (blue triangles), and stations with long-term records (green pentagons) are also shown.

Table 2.2 – Example time-series file for the 80-m wind at a single grid point. The first row indicates the latitude and longitude of the grid point. The other rows contain the data in the following columns: (i) date in YYYYMMDD format, (ii) time (UTC) in HHMM format, (iii) speed in m/s, (iv) direction in degrees from true north, (v) air density in kg/m³, and (vi) TKE in m²/s².

21.91430	-159.53020				
20070101	0010	8.43500	77.64800	1.15761	3.11400
20070101	0020	8.42600	78.47800	1.15707	3.48700
20070101	0030	8.38800	78.21900	1.15628	3.43700
20070101	0040	8.23400	74.05000	1.15626	3.51700
20070101	0050	8.16300	78.76700	1.15595	3.11000
20070101	0100	8.56800	72.15000	1.15648	3.26400
20070101	0110	8.34100	80.66200	1.15626	3.06000
20070101	0120	8.12900	73.86900	1.15658	2.93500
20070101	0130	8.06700	75.75200	1.15670	2.85500
20070101	0140	8.26700	73.27300	1.15688	2.93200
20070101	0150	8.29800	75.23700	1.15724	2.82800

3 Generating Wind Plant Output

3.1 Conversion Procedure

Converting the meteorological data generated by the mesoscale model to wind plant output was done by a program written by AWS Truepower called SynOutput.

The program starts by reading a list of five tall towers in the validation region and their nearest associated grid cells (grid number and column and row position). It also reads a list of the grid cells associated with the sites. Up to several dozen grid cells are associated with each site, depending on its size and shape. For each cell, the list provides the latitude and longitude, expected mean speed of the part occupied by turbines, mesoscale grid cell elevation, actual mean elevation of the turbines, and relative proportion of the site’s total rated capacity associated with that cell. The mean speeds are based on AWS Truepower’s proprietary Hawaii wind map¹. An example of 200-m map grid cells within 1-km model grid cells for a hypothetical site is shown in Figure 3.1. In locations with validation towers, the mean tower speed was compared to the mean map speed at the nearest grid cell, and the map speed at the grid cell was adjusted accordingly.

¹ The Hawaii wind map was generated at a horizontal resolution of 200 m, which is sufficiently fine to reflect the influence of most terrain features and identify specific locations for wind projects. AWS Truepower has developed a method of adjusting its wind maps using a wide array of wind resource measurements to ensure accuracy.

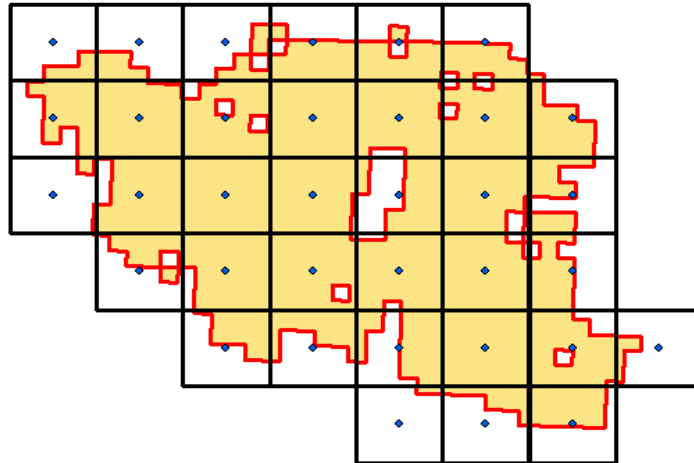


Figure 3.1 – Example of 200-m map cells within 1-km model grid cells for a hypothetical site.

The program then imports the turbine power curves. For the existing sites where turbine specifications were known, the turbine power curve was used. For all other sites, a composite power curve was created reflecting the estimated IEC site classification. There is one power curve for each IEC class (Table 3.1.) The power curves are scaled to a rated capacity of 2 MW and are valid for the standard sea-level air density of 1.225 kg/m^3 . The IEC 1 and 2 curves are based on a composite of three commercial turbines (General Electric/GE, Vestas, and Gamesa brands). In consultation with NREL, it was decided to base the IEC 3 curve on just two turbines (GE 1.5xle and Gamesa G90) to avoid an inconsistency in the cut-out speed of the Vestas V100. In addition, the cut-out speed of the GE turbine was changed from 20 to 21 m/s to match that of the Gamesa turbine. The IEC 1 and 2 turbines are assumed to have a hub height of 60 m and the IEC 3 turbine 80 m. Due to the low shear environment in Hawaii, it is assumed that the lower hub height will be used unless the wind resource dictates moving to a higher hub height to capture enough wind.

The program next reads a set of 12x24 speed matrixes, one for each of the validation towers. These matrixes give the mean speed for each hour of the day and for each month of the year. For each tower there are two matrixes, one for each hub height (60 m and 80 m). The program reads the mesoscale time-series file for each of the grid points nearest the validation towers. From the speed data, it creates a 12x24 mean speed matrix for each hub height. The ratio between the average observed and average simulated speed is then calculated for each bin and normalized to an average of one. The result is an adjustment matrix which is used to correct model biases. Although the program calculates adjustments on a monthly basis, it was found during the validation phase that the monthly variation in speeds was accurately predicted by the model. Therefore, only an annual adjustment is actually performed.

The mesoscale time-series files are then read for each grid cell associated with a project site. The speed data are scaled to match the expected mean speed and finally summed for all the grid cells associated with the site. In the sum, each cell's speeds are weighted according to the proportion of the site area associated with that cell. The result is a time series of simulated wind speeds for the site as a whole at both 60 m and 80 m.

Table 3.1 – Composite power curves for IEC Class 1, 2, and 3 turbines at standard air density (1.225 kg/m³).

Speed (m/s)	Power (kW)		
	IEC-1	IEC-2	IEC-3
0	0	0	0
1	0	0	0
2	0	0	0
3	0	0	12.6
4	39	56.6	82.4
5	136.2	176.8	204
6	280.2	347.8	378
7	474.2	574.6	621.4
8	732.6	867.8	943
9	1046.6	1213.2	1325.8
10	1404.2	1553.6	1676.6
11	1712.8	1810	1892.8
12	1911.2	1943.4	1974.2
13	1974.8	1985.2	1995.2
14	1989	1995.8	1999
15	1996.4	1999.6	1999.8
16	1998	2000	2000
17	2000	2000	2000
18	2000	2000	2000
19	2000	2000	2000
20	2000	2000	2000
21	2000	2000	2000
22	2000	2000	0
23	2000	2000	0
24	2000	2000	0
25	2000	2000	0

The program calculates a correlation coefficient (r^2) between the simulated daily mean speeds for the site in question and the simulated daily mean speeds for each validation location. It then calculates a weighted average adjustment matrix for the site in which the weight given to the adjustment matrix for each validation location is proportional to its correlation coefficient. The program applies this blended adjustment matrix to the simulated data for the site. For example, if the time in question is 1300, the simulated speed is multiplied by the adjustment factor for 1300.

The speed at each grid point is then adjusted for wake losses in a manner that depends on the simulated wind direction relative to the prevailing (most frequent) direction. The loss is given by $w = w_{\min} + (w_{\max} - w_{\min}) \sin^2(\theta - \theta_{\max})$, where w_{\min} is the minimum loss (assumed to be 4%) when the wind is aligned with or opposite to the prevailing direction θ_{\max} , and w_{\max} is the maximum loss (9%) when the wind is perpendicular to the prevailing direction. The loss factors account both for wake losses and implicitly, for other losses such as blade soiling, that affect the efficiency of power conversion for a given free-stream speed without reducing the maximum

output. These losses were determined by trial and error to conform to AWS Truepower’s estimates for actual wind projects. The method does not account for sites where there is more than one prevailing wind direction or where the prevailing energy-producing direction differs from the most frequent direction. However, the wind direction distribution was found to be unimodal at the sites of interest in this study.

The speed is further adjusted by adding a random factor (from -1 to +1) multiplied by the predicted TKE. This adjustment is intended to reflect the impact of gusts on the speeds experienced by the turbines in the wind project. The frequency and intensity of such simulated gusts depends to a degree on time of day, because TKE is generally higher in the day when the planetary boundary layer is thermally unstable or neutral compared to night when it is thermally stable.

Next, the adjusted speed for each grid cell is applied to the turbine power curve for each IEC class. In the process, the power curve is corrected to the predicted air density. A time filter is then applied to mimic the effect of spatial averaging on the fluctuations of wind output over the area of a mesoscale grid cell. The time filter gives a weight of 90% to the predicted output at the current time, and divides the remaining 10% weight equally among the predicted output values of the previous 17 time records (i.e., about three hours of actual time). This approach has been found to reproduce the observed “variability” of wind plant output, as measured by the mean absolute deviation (MAD) as a function of time, with reasonable accuracy.

The program applies an additional power loss to account for turbine and plant availability. Based on data obtained by AWS Truepower for operating wind projects, the availability is assumed to follow a normal distribution with a mean of 94.8% and a standard deviation of 2.3%; the distribution is truncated at 100%. To avoid unrealistic rapid fluctuations in output, the availability is allowed to change at random intervals averaging only once per hour. An additional loss of 3% is subtracted from the output to represent electrical losses.

In order to facilitate multiple capacity scenarios at various sites, NREL requested output for each 1-km grid cell as well as for each aggregated site. Therefore, the simulated speeds at both hub heights and the power output for all IEC classes are output to a single text file for each site, as well as each individual grid point within a site. In addition, the program selects the most appropriate IEC class based on the estimated maximum long-term annual mean speed within the site based on the Hawaii wind map, adjusted for air density. The same IEC class is selected for each point within a site. The power output for the selected IEC class is provided in the last column of the file. A sample text file of site output is shown in Table 3.2.

Table 3.2 – Sample plant output data file. The selected output column corresponds to the IEC class of the site, in this case IEC Class 3.

SITE NUMBER: 4403 RATED CAP: 100.2 IEC CLASS: 3 LOSSES (%): 19.5 18.6 17.0							
Date	Time (UTC)	Speed (60 m)	Speed (80 m)	IEC1 (60 m)	IEC2 (60 m)	IEC3 (80 m)	Selected
20070101	10	3.876	4.062	1.2	1.8	3.3	3.3
20070101	20	3.982	4.314	1.4	2.0	4.2	4.2
20070101	30	4.844	5.204	4.0	5.3	8.3	8.3
...

3.2 Validation

NREL, in collaboration with the Hawaiian Electric Company (HECO), provided approximately two years of 2-second plant output data for one project within Hawaii; KWP1 on the island of Maui. A 10-minute time series over the 2-year period was created by extracting the instantaneous 10-minute values to facilitate comparison between modeled and observed data. One year of power and nearly six months of speed data with a 15-minute frequency from two other plants in Hawaii (HRD and Apollo, both on the island of Hawaii) were also provided. Table 3.3 lists the period of record and data frequency for the three plants.

Table 3.3 – Plants with historical data.

Plant Name	Island	Speed POR	Power POR	Data Frequency	Validation Interval
KWP1	Maui	17 Oct 06–	17 Oct 06–	2 sec	10 min
		26 Aug 08	26 Aug 08		
HRD	Hawaii	23 Jul 08–	1 Jan 07–	15 min	30 min
		31 Dec 08	31 Dec 08		
Apollo	Hawaii	23 Jul 08–	1 Jan 07–	15 min	30 min
		31 Dec 08	31 Dec 08		

Initial validation of diurnal patterns at KWP1 revealed a deficit in observed power during the overnight hours. By calculating the power output using the observed wind speed and the actual turbine power curve, it was concluded that this deficit must arise from nighttime curtailment of the plant (Figure 3.2). Since it is assumed that system constraints dictate nighttime curtailment, modeled data will not replicate this behavior. For validation purposes, periods of curtailment must be removed to create a more accurate comparison between observed and modeled data.

A curtailment log file at KWP1 for 2007 was obtained from HECO by GE and forwarded to AWS Truepower for use in the validation. Any period either flagged as curtailed or missing curtailment information was removed from both the observed and modeled power data. This process eliminated 22.8% of the 2007 data.

At HRD, the plant limit was available for a portion of the period. When the plant limit was less than 95% of the rated capacity, curtailment was assumed and the power output was removed from both the observed and modeled data. Eliminating periods of curtailment or missing plant limit information removed 28.8% of the data.

Apollo is divided into two groups of turbines. Both the plant limit and the group limit were available for a portion of the period. When either the plant limit or the sum of the group limits was less than 95% of the plant rated capacity, the power output was removed from both the observed and modeled data. Power output was also removed any time when curtailment information was unavailable. These criteria removed 46.9% of the records at Apollo. Table 3.4 lists the period of record and the percentage of records within this period removed.

The power conversion program was tested using mesoscale data extracted for grid points associated with KWP and Southeast Maui sites. As a result of the initial validation, the time filter was eliminated and the modeled wind speed variability was increased using a TKE-based parameterization. The results were presented to NREL in both tabular form and as diurnal and monthly change plots.

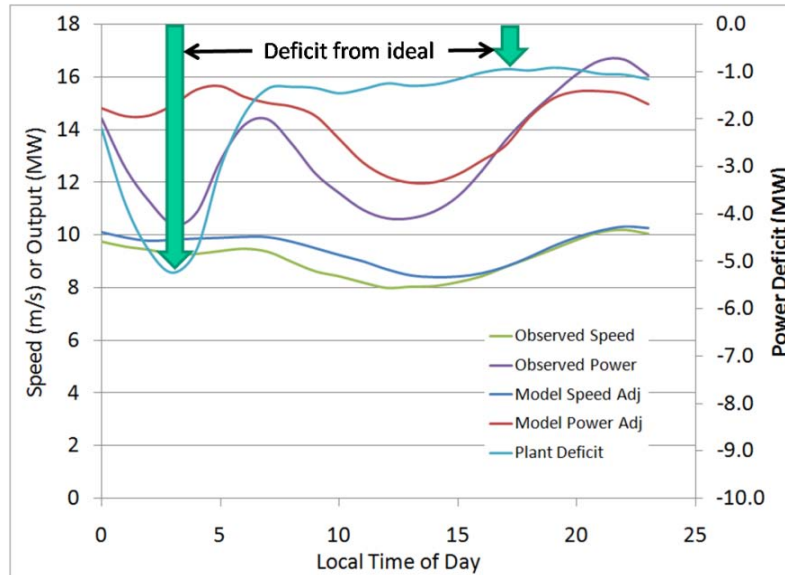


Figure 3.2 – Observed and modeled power output and wind speed at KWP1. The cyan line marks the difference between idealized power output (calculated by running the observed winds through the actual turbine power curve) and observed power output.

Table 3.4 – Period of record after periods of curtailment were removed.

Plant	Speed POR	Power POR	% Removed
KWP1	0010 UTC 1 Jan 07–	1350 UTC 2 Jan 07–	22.8%
	0850 UTC 27 Aug 08	0840 UTC 1 Jan 08	
HRD	1830 UTC 23 Jul 08–	0900 UTC 27 Mar 08–	28.3%
	0000 UTC 1 Jan 09	0000 UTC 1 Jan 09	
Apollo	1830 UTC 23 Jul 08–	1730 UTC 3 Jul 08–	46.9%
	0000 UTC 10 Oct 08	0000 UTC 1 Jul 09	

As noted previously, significant jumps in wind speed can occur at 0000 and 1200 UTC. AWS Truepower concluded that the jumps were caused by the abrupt assimilation of rawinsonde and surface observations every 12 hours in the mesoscale runs. A workaround was developed in which values spanning the affected times were replaced with synthesized data (Figure 3.3). This workaround was deemed sufficient for EWITS and was thus used for the Hawaiian Islands study.

Additional issues were identified with the mean absolute changes in 10-minute wind speed and power output in comparison with observed values at KWP1. The software was modified to address these issues. First, the wind speeds were smoothed with a 1-2-1 filter. The difference between the original and smoothed speeds was saved as a residual. A scaled 10-minute wind speed change, randomly sampled from the residuals, was then applied to each wind speed. In this way, the integrity of the original time series as well as the statistical behavior of the variability was preserved, while the unrealistic jump in wind speed near 1200 UTC was removed. Figure 3.4 shows the mean absolute change in wind speeds observed at KWP1 compared with results before and after the adjustments were applied. With these revisions, the plant output data files were generated and delivered to NREL.

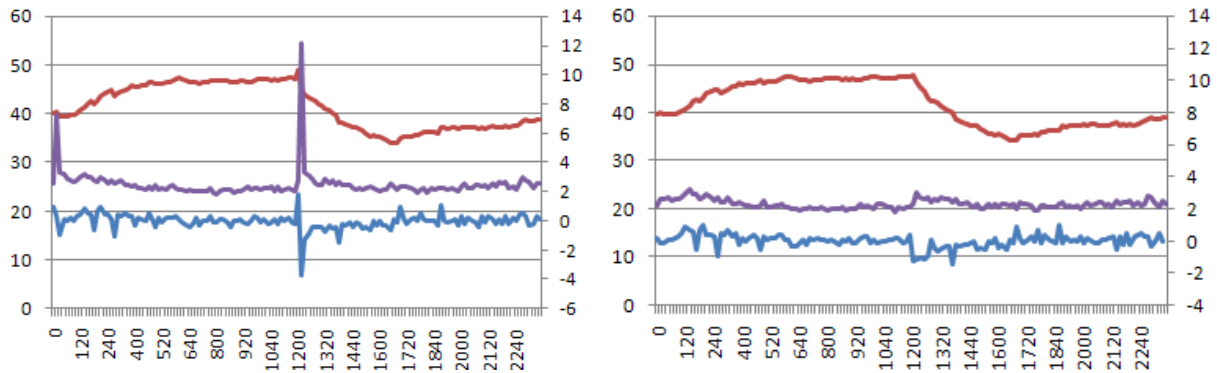


Figure 3.3 – Jumps in mean speed at one site before (left) and after (right) the fix. The red curve is the mean output (left axis), the purple curve is the absolute change in output from one 10-minute record to the next (left axis), and the blue curve is the change in output (right axis).

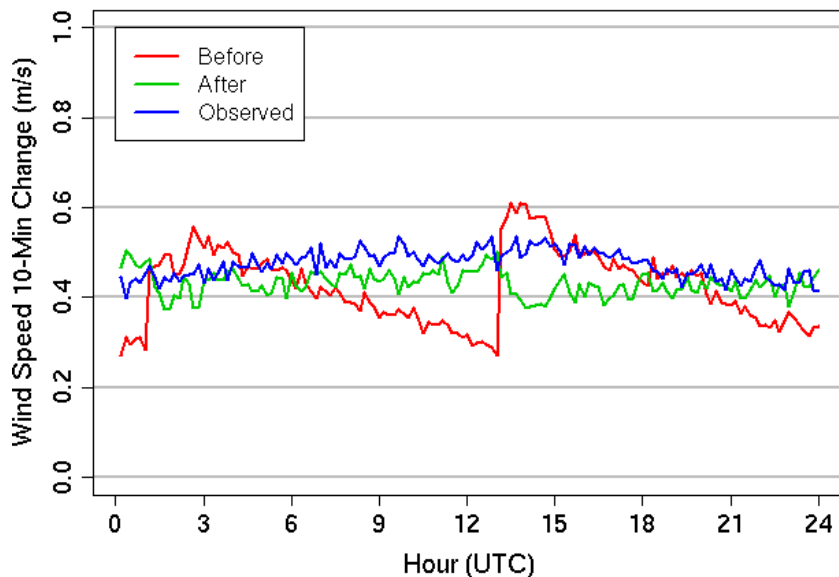


Figure 3.4 – Ten-minute mean absolute change in wind speed at KWP1 before adjustment (red), after adjustment (green), and observed (blue).

By employing an appropriate turbine power curve for each project, adjusting the hub height of the simulated speeds and diurnal corrections to match the actual hub height, and removing curtailments from the observations, a reasonably close agreement between the predicted and observed net capacity factor and diurnal patterns was obtained at the three validation projects (Figure 3.5). Diurnal wind speed comparisons, as well as monthly patterns in wind speed and capacity factor, can be found in Appendix Figures A.1 and A.2. The distribution of ramps in power output was also compared (Figure 3.6). Similar plots on a linear scale can be found in the Appendix (Figure A.3). The distribution of power ramps agrees well at KWP1, where the period of record was substantial and curtailments were a minimum. Ramps at HRD and Apollo are less comparable due to the limited period of record during which curtailments were common. Time series of power output at these two sites revealed that output remained near maximum capacity for extended periods, creating unrealistically low variability. A table of ramp statistics for each site can be found in the Appendix (Table A.1).

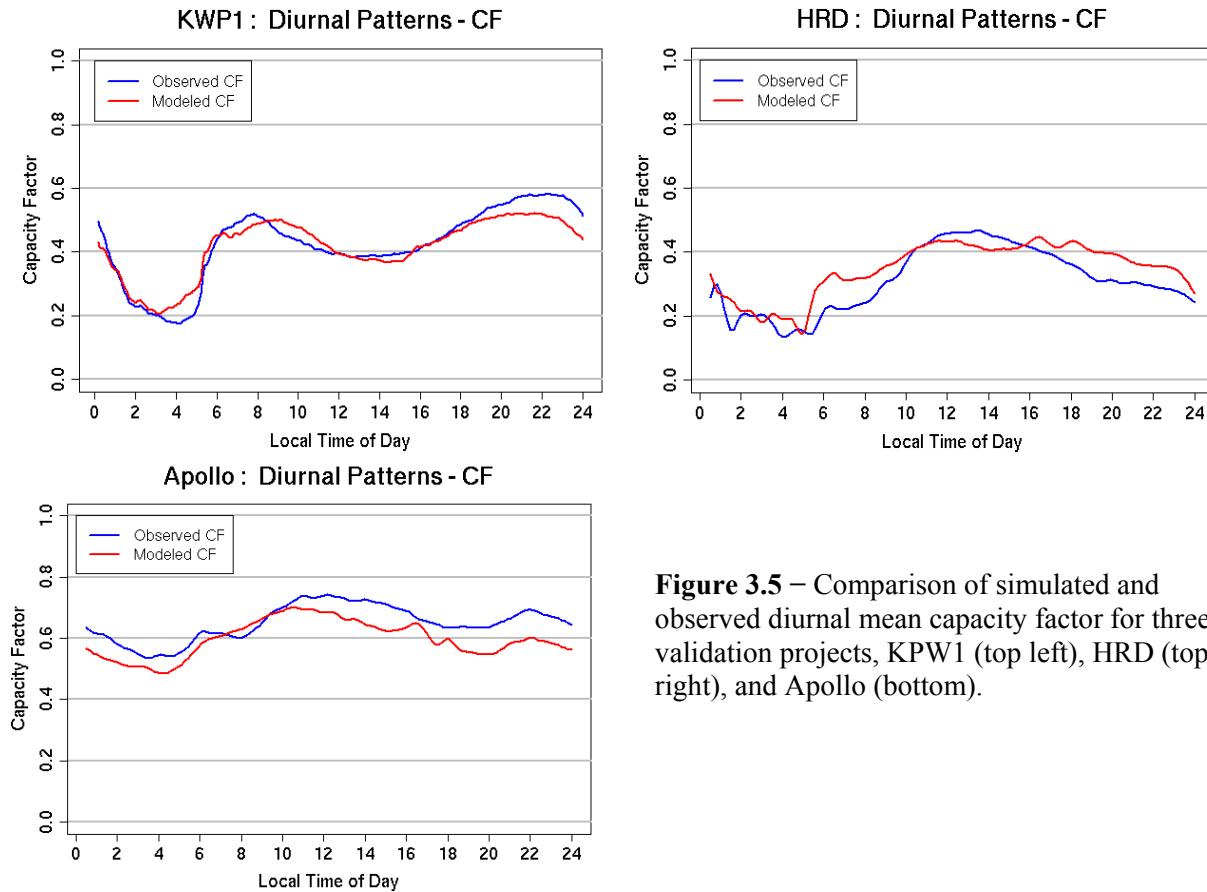


Figure 3.5 – Comparison of simulated and observed diurnal mean capacity factor for three validation projects, KPW1 (top left), HRD (top right), and Apollo (bottom).

Modeled and observed wind speeds were also compared at the five validation towers, with figures shown in the Appendix.² The diurnal and monthly wind speed patterns at the validation towers followed those at nearest 1-km grid points with reasonable accuracy (Figures A.4 through A.8). The distribution of 10-minute changes in wind speed were also compared. As expected, it was found that wind speeds at towers closest to the model grid-point location and elevation validated better than those towers well outside of a modeled site. In addition, the observed winds were more variable than raw simulated winds, which is why the TKE adjustment was applied to the wind speeds before generating power output.

Observed and modeled monthly and diurnal mean winds were compared in 2007 versus 2008. Tall tower and surface observations (sites shown by green pentagons in Fig. 2.2) showed that 2007 was windier than 2008. Neither year differed substantially than the long-term climatology based on buoy data (Figure 3.7). The simulated means from all sites captured this trend.

NREL personnel noted that simulated power output did not reach plant capacity, whereas observed output does reach such levels at KWP1. This issue was traced to the fact that the randomly-generated availability loss was applied separately to the output data for each grid point. The method was adjusted so that the same availability loss was applied to every grid point in a site. At the same time, an underrepresentation of wind speeds on the island of Lanai was discovered by NREL and AWS Truepower. The map speeds were scaled up to available observations, and an updated dataset was generated and delivered to NREL.

² The location of the tall towers is proprietary, and therefore not disclosed in this report.

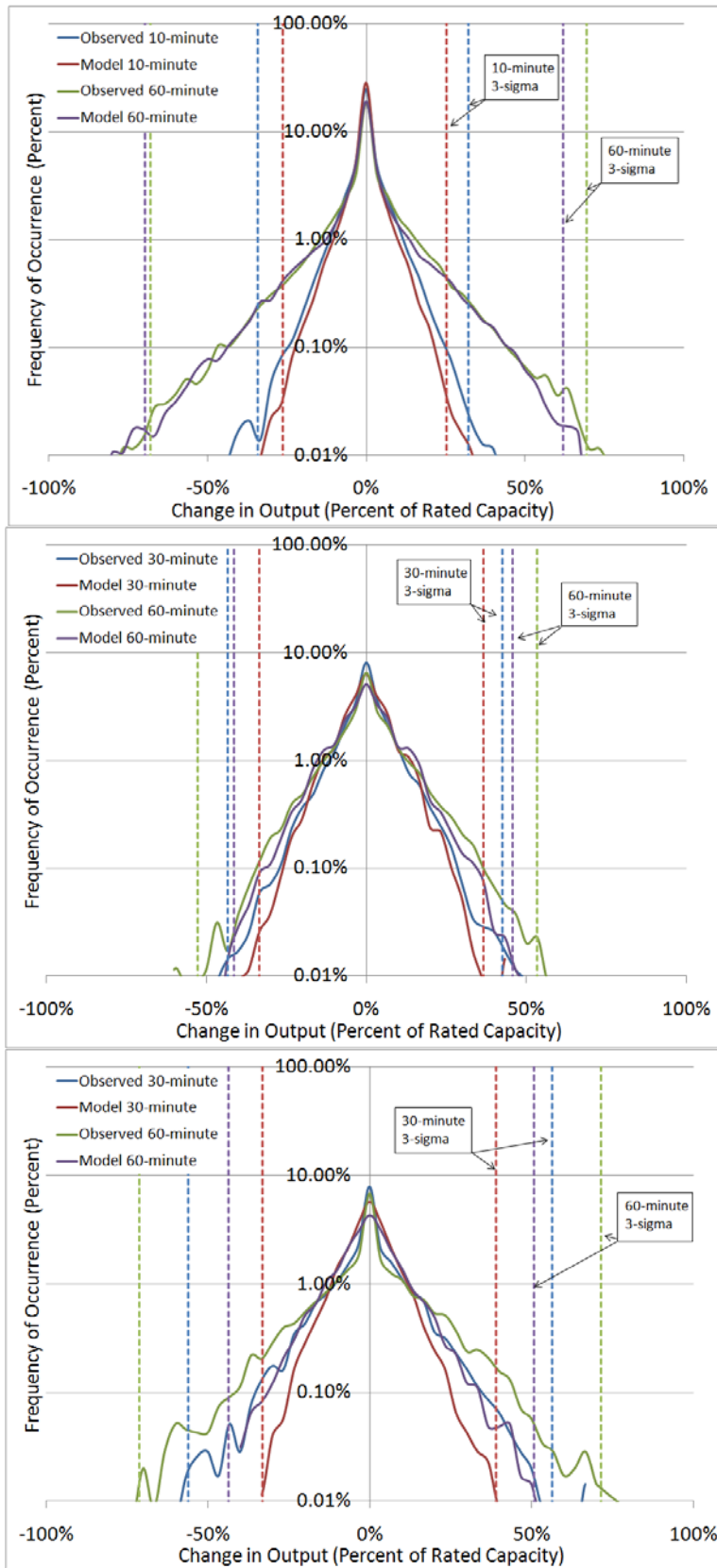


Figure 3.6 – Comparison of simulated and observed power ramps for KPW1 (top), HRD (middle), and Apollo (bottom).

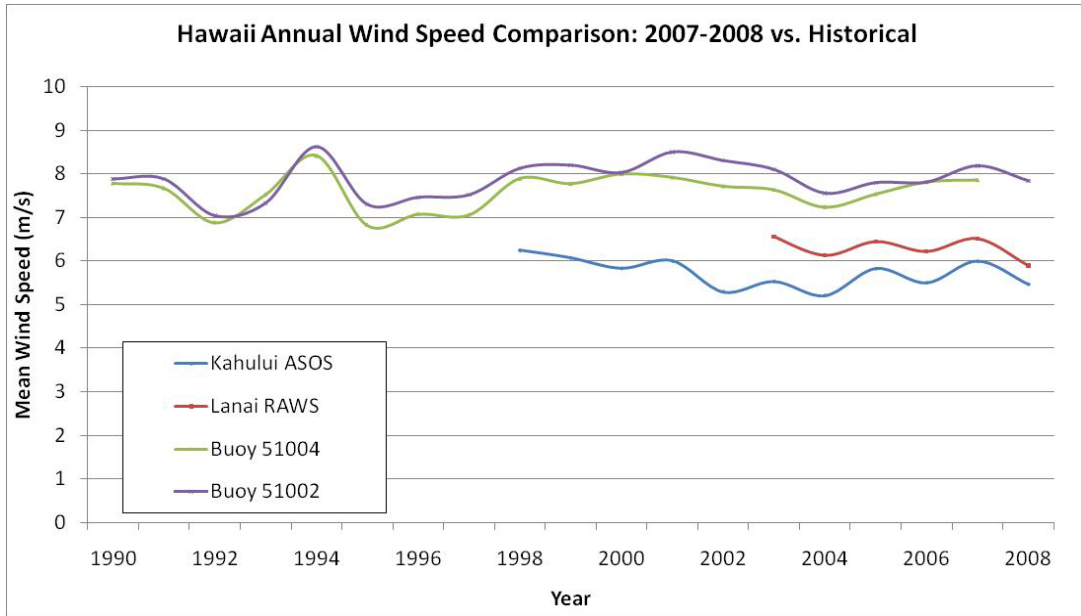


Figure 3.7 – Comparison of annual mean observed wind speeds for stations with long-term data (locations shown by green pentagons in Fig. 2.2).

3.3 Impacts of Model Restart/Assimilation

NREL discovered that modeled wind speed and power output experienced a large down ramp event on 15 October 2007. The time of this down ramp coincided with the MASS model restart (every 15 days) at which time the NNGR (NCEP/NCAR Global Reanalysis, NCEP/National Centers for Environmental Prediction, NCAR/National Center for Atmospheric Research) analysis is used for first guess and boundary conditions. The ramp event was also coincident with the assimilation of rawinsonde observations in the model at 12-hour intervals. In order to determine whether the model restart with NNGR data and/or rawinsonde assimilation impacted the down ramp, AWS Truepower executed two additional MASS simulations starting 14 October, 2007, and ending 17 October, 2007. Table 3.5 summarizes the differences between these runs.

Table 3.5 – Summary of model restart/assimilation runs.

Run Name	Assimilation	Restarted 0000 UTC 16 Oct
ASSIM (production run)*	Yes	Yes
ASSIM/NO-RESTART	Yes	No
NO-ASSIM/NO-RESTART	No	No

*Completed as part of primary modeling effort.

Time series of 80-m wind speed from the three runs were compared at sites 1-6 (Maui), 13 (Lanai), and 20-23 (Molokai). Figure 3.8 shows the large decrease in wind speed at 0000 UTC 16 October in the production run (blue line) at all three locations. When the model was not restarted with the NNGR data, no such decrease in wind speed occurred with or without the assimilation of rawinsonde (green and red lines, respectively). The results show that the model restart with NNGR data on 16 October, 2007, was the cause of the large decrease in wind speed, and ultimately the large down ramp in power at this time. On the other hand, the assimilation of rawinsonde data was not a factor in causing this ramp event.

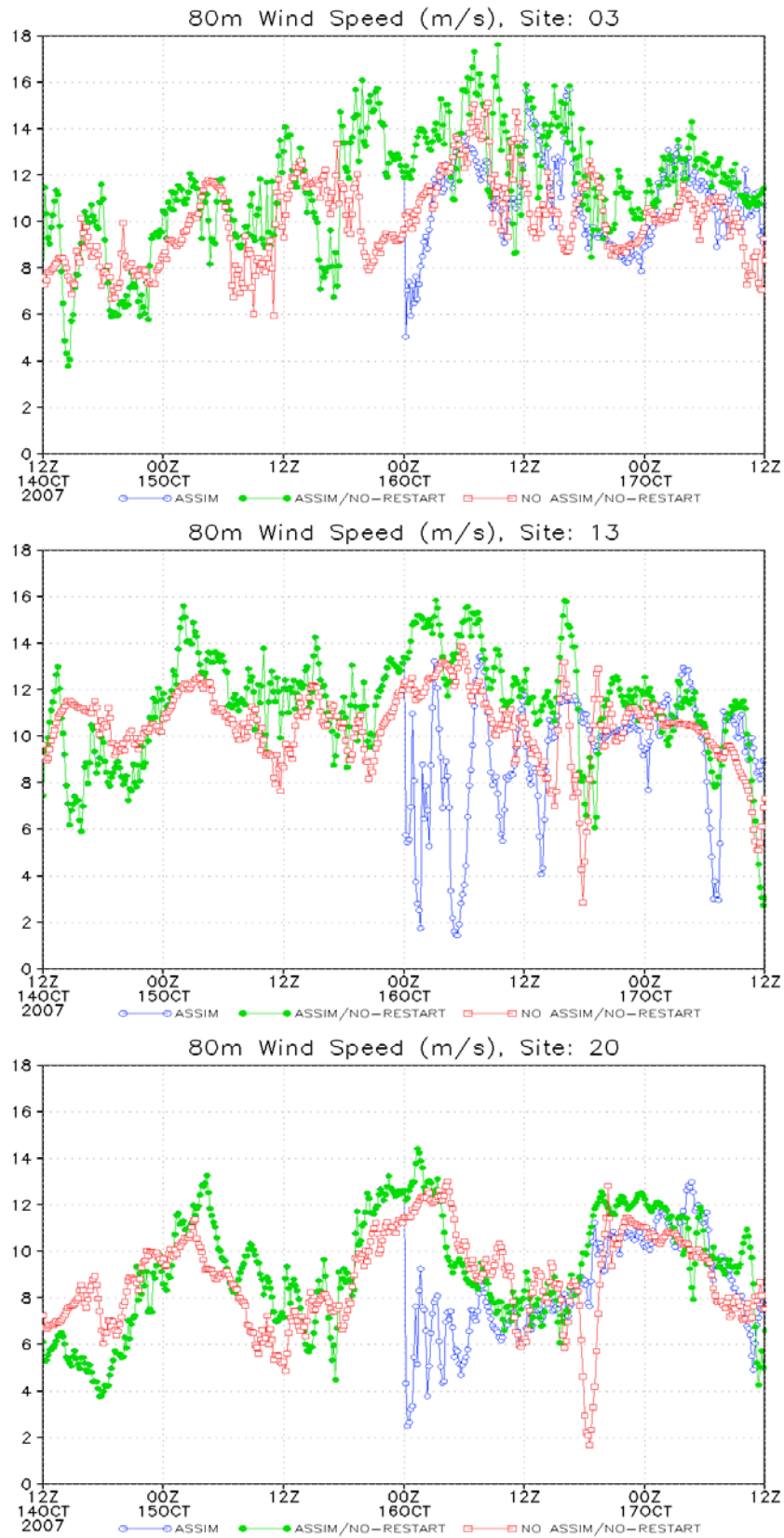


Figure 3.8 – Comparison of 80-m wind speeds from three different model runs: original run with data assimilation (blue), data assimilation with no NNGR restart (green), and no assimilation/no restart (red).

4 Forecasts

AWS Truepower produced hourly forecasts for four different time horizons: next-day, six-hour, four-hour, and one-hour. Each set of forecasts was synthesized by running a statistical forecast synthesis tool written by AWS Truepower called SynForecast. This tool uses actual forecasts and observed plant output to develop a set of transition probabilities, which are then applied stepping forward in time from a random starting point in a process known as a Markov chain. The procedure is described in depth in the following section.

4.1 Forecast Synthesis Procedure

The first step in the forecast synthesis process is to produce a sequence of real forecasts for one or more operating wind projects using a state-of-the-art wind forecasting system. It is assumed that these forecasts are typical or representative of forecasts at other sites in the region. For this purpose, AWS Truepower ran its *eWind* forecasting system³ in “hindcast” mode for the three wind plants for which NREL had previously provided output data for 2007-2008: KWP1, HRD, and Apollo. Sufficient wind speed and power output data was available at KWP1 to generate model output statistics (MOS) using simulated and observed wind speeds. Since wind speed data was limited to less than six months at HRD and Apollo (see Table 3.4), a direct wind speed to power output MOS was used at these sites. In this case, the eWind statistical module transformed the mesoscale model data directly into plant output via an implicit non-linear power curve derived from data for the preceding 30 days of actual and simulated output. AWS Truepower determined that the large number of curtailment and site unavailability events combined with the small sample size prevented the eWind system from generating an adequate MOS for Apollo. Therefore, only model training data from KWP1 and HRD were used to generate the forecast data.

The mesoscale model feed for the forecast was provided by 4-km resolution MASS simulations. The observed data feed was provided by the actual plant data up to the time each forecast was assumed to be generated. For the 1-, 4-, and 6-hour forecasts, the latest time was one, four, and six hours ahead of the forecast valid time, and a new forecast was generated every hour with updated plant data. For next-day forecasts, the latest time was 8 am Hawaii local time, and forecasts valid from 7 pm to 6 pm the next day were generated once per day and appended to one another to form a continuous time series of forecasts.

From each of these four sets of forecasts, the SynForecast program constructed a matrix of forecast probabilities of the following form:

$$P(A_t \cap F_{t-1} \cap F_t)$$

The probability P is the number of occurrences for which the actual output was A_t and the forecasted outputs were F_{t-1} and F_t , where t is a particular moment in time and $t-1$ is the previous moment (one hour earlier). Before constructing this matrix, both the actual and forecasted output values were normalized to the rated capacity of the wind project and placed in ten bins ranging in capacity factor from 0.05 to 0.95 in increments of 0.10. Both the current and previous forecasts

³ eWind is a commercial wind forecasting service that uses weather forecasts from a mesoscale model, actual plant operating data, and on-site wind observations when available. Over a period of several days or weeks, eWind builds a statistical model relating the forecasted plant output to the actual plant output. This model is then applied to correct the wind forecasts going forward. Over time, the model “learns” from past forecast errors and its skill gradually improves.

are included in the probability matrix to capture the autocorrelation of forecast errors; otherwise, the synthesized forecasts would fluctuate randomly about the actual output in an unrealistic fashion.

For each wind project site, the SynForecast program selected, at random, one of the two transition probability matrixes. Starting with a random seed, the program stepped forward in time taking random draws from the transition matrix. In this manner, an hourly next-day forecast was synthesized.

4.2 Validation

To verify that the program was working properly, the synthesized forecasts were compared with the actual forecasts for the three validation wind projects. First, the validation focused on the time correlation of the actual and forecasted generation and the root-mean-square (RMS) forecast error (Table 4.1). The RMS error depends in part on the average plant output, with more productive plants experiencing higher forecast errors as a fraction of rated capacity because they spend more time in the steeply sloping parts of their power curves.

Table 4.1 – Correlation of forecasted and actual output and RMS forecast error for synthesized and real (eWind) 1-hour, 4-hour, 6-hour, and next-day (ND) forecasts.

1-hour	Correlation (Pearson r)		RMS Forecast Error (CF)	
	eWind	SynFcst	eWind	SynFcst
Plant				
KWP1	0.96	0.97	0.11	0.10
HRD	0.93	0.94	0.11	0.10
Apollo	0.87	0.90	0.13	0.11
4-hour	Correlation (Pearson r)		RMS Forecast Error (CF)	
	eWind	SynFcst	eWind	SynFcst
Plant				
KWP1	0.80	0.83	0.24	0.22
HRD	0.75	0.80	0.19	0.18
Apollo	0.55	0.66	0.22	0.20
6-hour	Correlation (Pearson r)		RMS Forecast Error (CF)	
	eWind	SynFcst	eWind	SynFcst
Plant				
KWP1	0.76	0.76	0.26	0.26
HRD	0.69	0.73	0.21	0.20
Apollo	0.45	0.57	0.24	0.22
ND	Correlation (Pearson r)		RMS Forecast Error (CF)	
	eWind	SynFcst	eWind	SynFcst
Plant				
KWP1	0.69	0.52	0.30	0.36
HRD	0.54	0.42	0.25	0.27
Apollo	0.28	0.13	0.26	0.29

The next comparison considered the autocorrelation of the forecasts and forecast errors. The autocorrelation indicates the degree to which a particular parameter tends to persist over time. A parameter that typically changes little would have an autocorrelation factor of nearly one, whereas one that fluctuates randomly would exhibit an autocorrelation factor of nearly zero. Since the sample size was so limited at Apollo, this plant was excluded from the analysis.

The following figures indicate that the forecasts of the remaining two wind projects tends to be quite strongly auto-correlated over a period of one to several hours for each forecast period (Figures 4.1–4.2). The SynForecast program seems to capture the pattern of decreasing correlation with increasing time shift quite well, as shown by the decreasing height of the bars for each forecast time. The eWind and synthesized forecasts exhibit similar degrees of autocorrelation in each case. Autocorrelation of observed output is shown for comparison. Forecasts are more auto-correlated at 4-hour and 6-hour than 1-hour and next-day time periods at both sites. Autocorrelation of 1-hour forecasts are lower because these forecasts are highly dependent on the most recent observed data, which changes hourly, whereas 4- and 6-hour forecasts are more dependent on the model, which is generally smoother. The autocorrelation of forecast errors is considerably lower, particularly for the 1-, 4-, and 6-hour forecast periods.

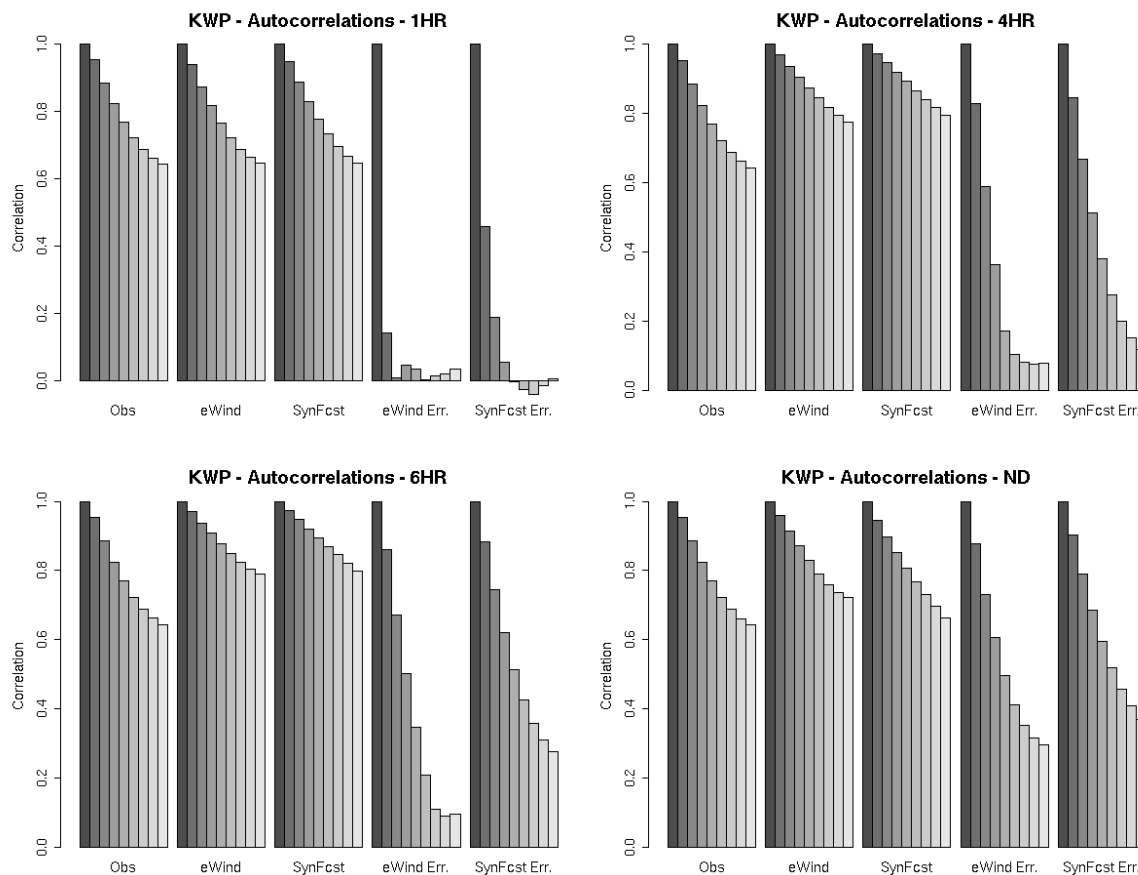


Figure 4.1 – Autocorrelation of observed output, eWind forecasts, synthesized forecasts, and forecast errors for increasing time shifts in hourly increments at KWP1. Autocorrelations are shown for one-hour (top left), four-hour (top right), six-hour (bottom left), and next-day (bottom left) forecasts.

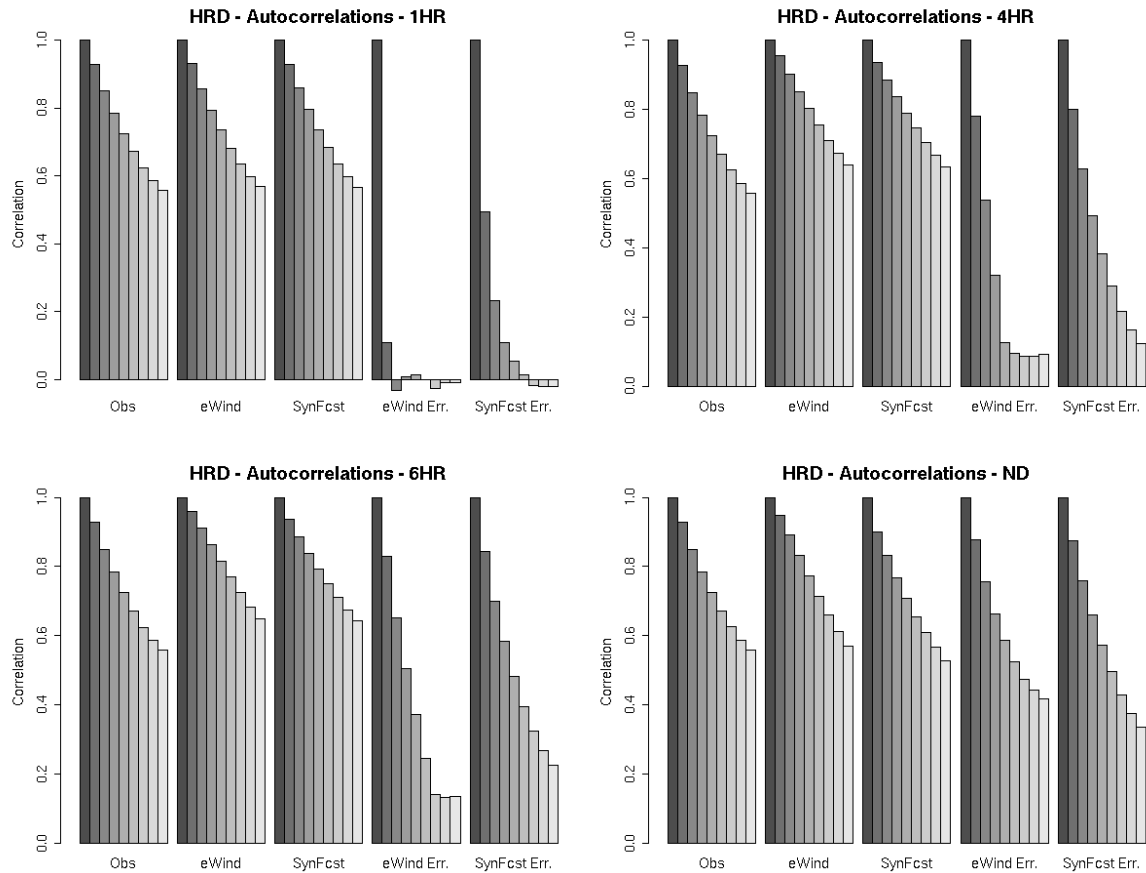


Figure 4.2 – Autocorrelation of observed output, eWind forecasts, synthesized forecasts, and forecast errors for increasing time shifts in hourly increments at HRD. Autocorrelations are shown for one-hour (top left), four-hour (top right), six-hour (bottom left), and next-day (bottom left) forecasts.

The correlation of forecast errors between projects as a function of distance between them is presented in Table 4.2. The limited number of projects with available data and questionable data at Apollo make it difficult to draw meaningful conclusions from these results. Unlike in EWITS, correlation of errors does not decrease with increasing distance between sites. cursory analysis suggests that sites that are farther apart but in similar flow regimes may be more highly correlated than closer sites in different flow regimes.

Table 4.2 – Correlation of output and forecast errors as a function of distance between project pairs.

Distance (km)	Sites	Observed Output	Modeled Output	eWind Error	SynFcst Error
96	KWP1-HRD	0.38	0.41	0.14	0.07
142	HRD-Apollo	0.45	0.39	0.08	0.23
224	KWP1-Apollo	0.24	0.10	0.03	0.03

5 High-Frequency Output

In the final task, AWS Truepower simulated 2-second plant output data at all sites for 2007 and 2008. To produce the data, AWS Truepower employed software to sample 40-minute windows of historical 2-second data from existing wind projects. The source of the samples was nearly two years of 2-second plant output at KWP1 and three days per month for one year at HRD and Apollo. Periods of curtailment were removed from the data in the same manner as described in Section 3.2. Even after removing curtailments, significant problems with HRD and Apollo data existed such that GE recommended excluding these two sites from the analysis. The remaining data quantity was sufficient for the study, to the extent that high-frequency behavior at KWP1 is representative of high-frequency behavior at other sites. Further evaluation is needed to determine whether the availability of quality data at other sites would improve the analysis.

The program removed 2-second trends from the remaining KWP1 data using a bicubic fitting procedure and then added the residuals to the simulated 10-minute output for each site. The residuals were scaled such that output at larger plants was less variable than at smaller plants. The algorithm did not allow the same window of residuals to be applied to two different sites in the same time period, as this would have resulted in perfect correlation of the 2-second fluctuations between those sites, whereas in reality 2-second fluctuations between wind projects are entirely uncorrelated. The program excluded all data from HRD and Apollo, any periods of curtailment, and 2-second changes greater than 5% of the plant rated capacity, as they likely correspond to plant outages, curtailments, and restarts unrelated to the wind that may have not been captured by the curtailment flag. A 1-minute dataset was then created by extracting instantaneous 1-minute values from the 2-second dataset.

Figure 5.1 shows a typical 24-hour sample of 2-second simulated and actual plant output for a single project overlaid on 10-minute data for the same site on the same day. Although modeled data from any given period may not exactly match observed data from same time period, the statistical behavior of the datasets (i.e., distribution of ramps) is comparable (see Figs. 5.3, 5.4).

The ramp distributions were compared to determine whether accuracy improved if samples were selected based on similar months or times of day. Choosing samples based on time of day had a negligible impact, while choosing samples from similar months showed a slight improvement in ramp agreement. Since the sample size was too small to choose for both time of day and month of year, it was decided to create the output with samples chosen from similar months only.

The high-resolution plant output data was reviewed by NREL using power spectral densities (PSD). Numerous peaks in the spectra were noted at high frequencies in the modeled data, whereas no such peaks were found in the observed data at KWP1. AWS Truepower concluded that the spurious peaks were caused by binning blocks of 2-second data based on season, thereby limiting the sample size. When samples were not chosen based on time of year, the spectral peaks disappeared and the PSDs of observed and modeled data were comparable (Figure 5.2). It was found that flattening of the spectrum in the 10 to 20-minute time periods was due to the statistical method used to correct the problem shown in Figure 3.4. Since the correction was necessary, it was determined that the discrepancies in the spectra were acceptable.

The resulting frequency distribution of step changes in simulated and actual 1-minute and 2-second output at KWP1 is shown in Figure 5.3. The distributions are reasonably similar. The asymmetry in 1-minute step changes is the result of KWP1 restricting up ramps to 2 MW per minute, while not restricting down ramps. Since KWP1 data is applied to all sites, an asymmetric

distribution of step changes was produced at each site. A workaround was developed such that the sign of the residuals was randomly reversed in blocks with step changes greater than or equal to 1.5 MW per minute. The modification resulted in a more realistic, symmetric distribution of step changes (Figures 5.4–5.5). With these revisions, the final high-frequency dataset was regenerated and delivered to NREL.

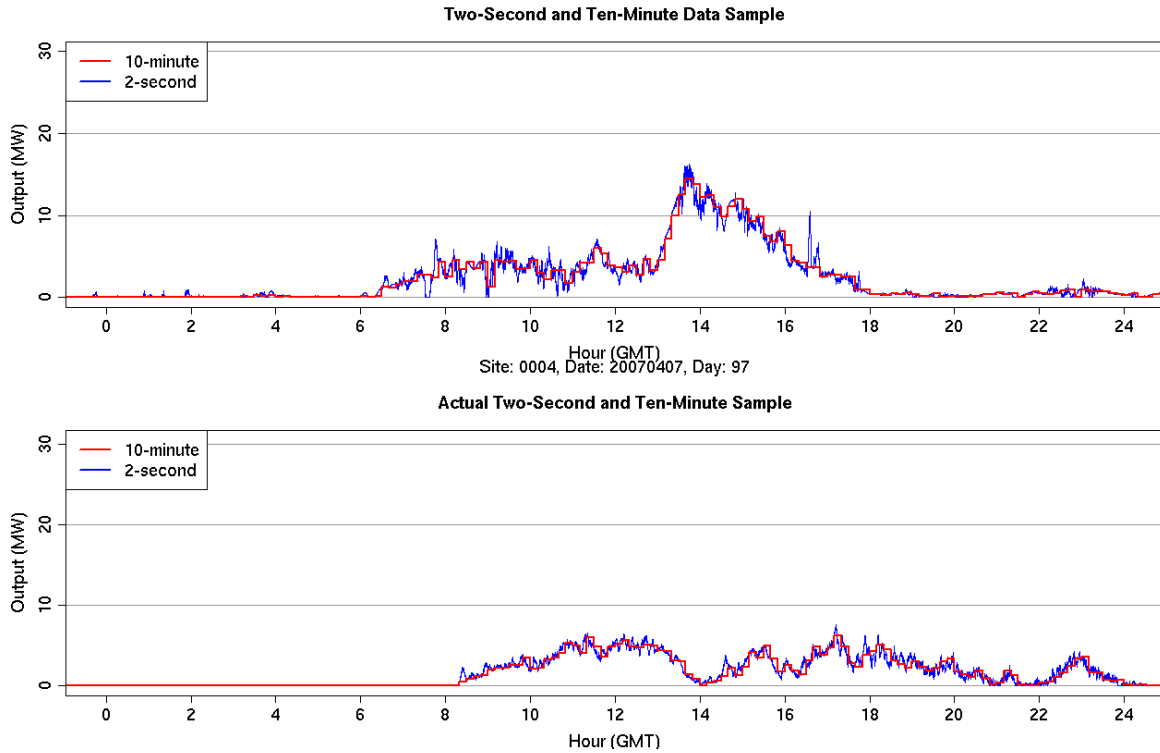


Figure 5.1 – One day of 2-second output (blue line) overlaid on corresponding 10-minute output (red line). The top chart shows simulated data for KWP1, while the bottom chart shows actual data.

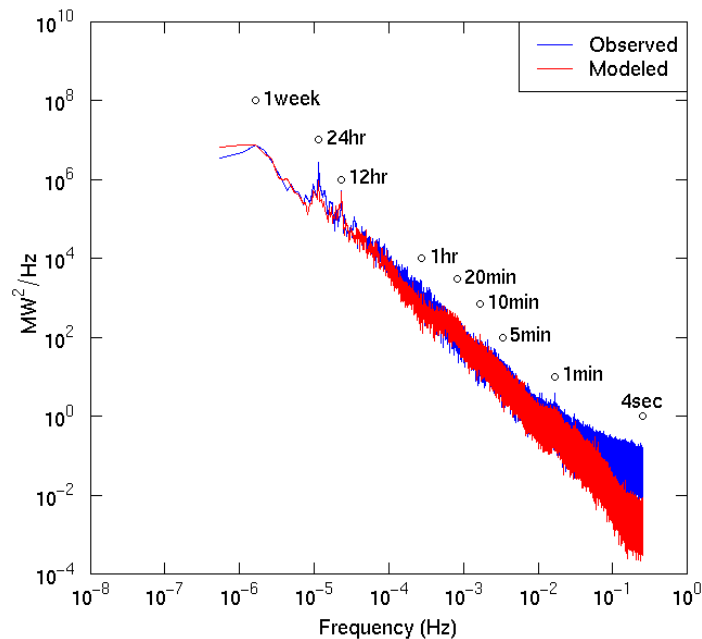


Figure 5.2 – Power spectral density of observed (blue) and modeled (red) high-frequency data at KWP1.

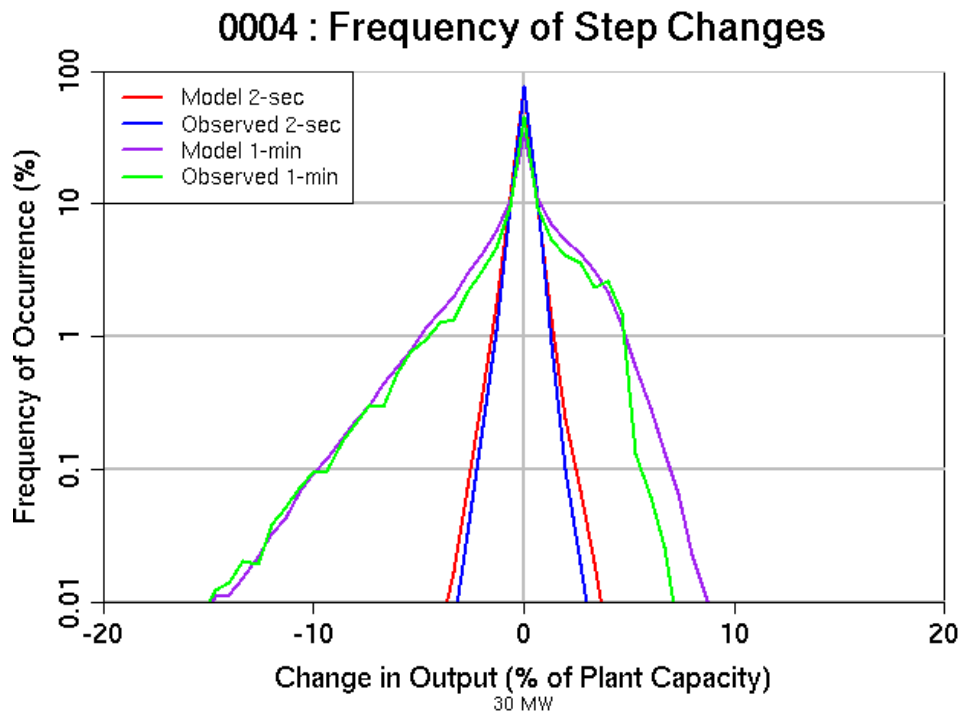


Figure 5.3 – Frequency distribution of step changes in simulated and actual 1-minute and 2-second output from 0000 UTC 1 Jan. 2007–1000 UTC 27 Aug. 2008 at KWPI.

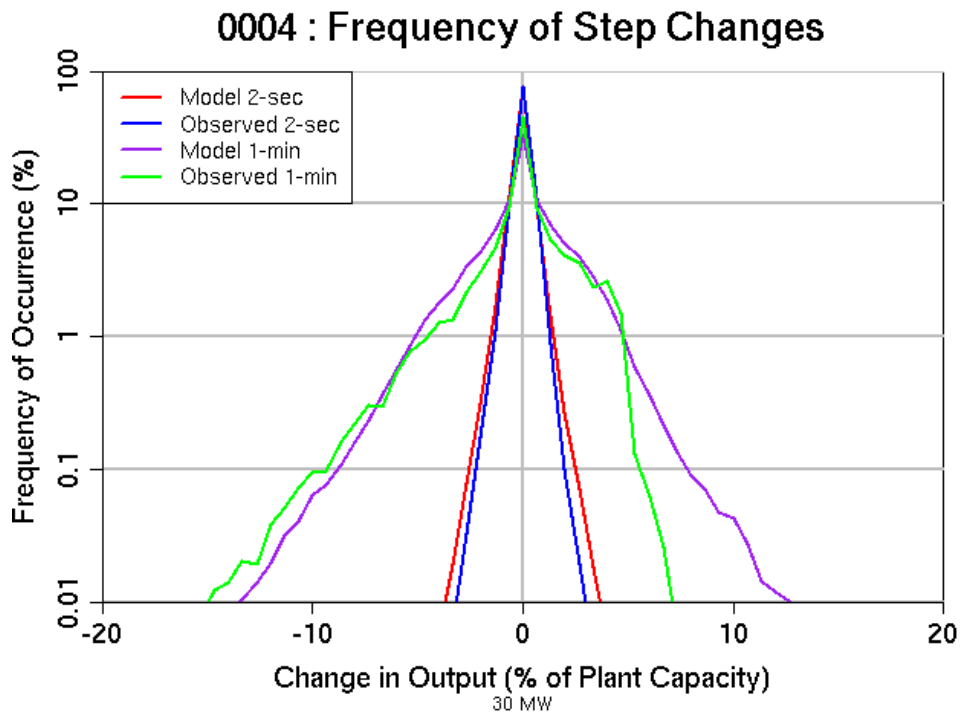


Figure 5.4 – As in Figure 5.3, but after workaround to correct asymmetry.

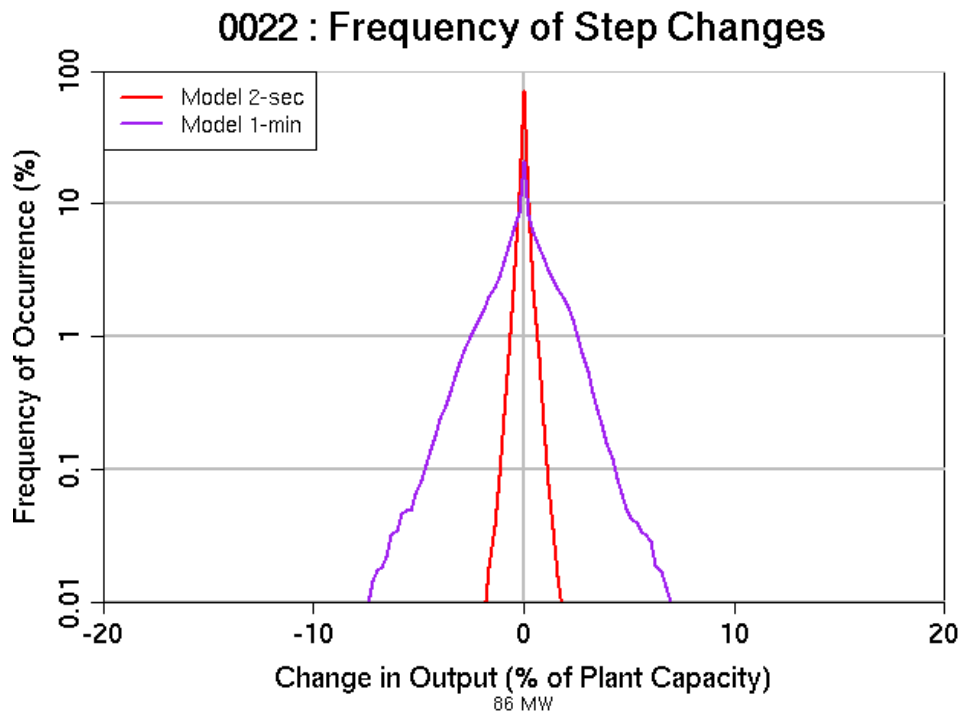


Figure 5.5 – Frequency distribution of step changes in simulated 1-minute and 2-second output from 0000 UTC 1 Jan. 2007–0000 UTC 1 Jan. 2008 at Site 22 after workaround to correct asymmetry.

6 Dataset Usage

The dataset was developed specifically for use in wind integration and transmission studies. Datasets were reviewed by NREL and members of the OWITS Technical Review Committee (TRC) set up to support HECO. Because variability is the key operational issue in integrating high penetrations of wind onto a power grid, the goal was to capture this feature as accurately as possible. The ramp histograms in Figure 3.6 were therefore a key part of the validation exercise. Spatial and temporal correlations between sites were also important metrics. This dataset focuses less on matching the absolute wind power output or capacity factor of any given site, but rather attempts to match the relative changes in these metrics across time and space.

Because the raw mesoscale-model wind-speed output does not include TKE, it is important for users to add that component, as described in Section 3.1 to properly account for variability associated with wind gusts.

Additionally, this dataset specifically models 2007 and 2008 but does not represent long-term averages that would be needed to ascertain the viability of projects at given sites. Long-term average wind resource maps (see <http://hawaii.gov/dbedt/ert/winddata/>) were produced by AWS Truepower using a similar methodology, but at a 200-m resolution, and represent a 10-year average wind resource.

Finally, it should be noted that modeled data is not a replacement for onsite measurements, and should not be used as the only basis for investment decisions.

7 Accuracy Summary

Extensive validation was undertaken to ensure accuracy of the dataset, with a focus on the ramping behavior. Wind speeds from KWP1 (Maui), HRD (Hawaii), Apollo (Hawaii), and five tall towers in the region were used to validate the model output speeds. Diurnal and monthly mean wind speeds validated well against observations at nearly all sites examined. Relative and absolute deviations in wind speed at 10-minute intervals also compared well with observed values, with the model data exhibiting a small low bias and stronger diurnal signal. It was noted that variability could be slightly higher than usual at 0000 and 1200 UTC due to the assimilation of observations.

The power conversion methodology underwent technical review through the Hawaiian Islands study project, and reasonable agreement was obtained for net capacity factors and diurnal and monthly patterns at KWP1, HRD, and Apollo. It should be noted that curtailment and missing plant information eliminated a significant amount of data that could be used in the validation of ramping characteristics. Apollo was not used in this analysis due to lack of quality data. Ramp statistics compared very well against observations for KWP1 and HRD after curtailment of existing plants was taken into account. In this dataset, the 3-sigma 10- and 60-minute variability matched the observed power ramps within 6-8% and 2-12%, respectively.

No model is a perfect reflection of reality. However, independent validation at AWS Truepower and NREL confirmed that the data reflect realistic averages, seasonal and diurnal patterns, and probability of ramping behavior for wind speed and power production in Hawaii.

8 Recommendations for Future Work

The following issues should be addressed in future studies:

- Validate wind and power output profiles initially developed in this study with on-site measurements from new plants when they are built;
- Determine whether forecast correlation depends more on distance between sites or location within similar flow regimes as actual plant data become available at additional sites;
- Compare high-frequency ramp statistics using other site versus only KWP1 data to determine if accuracy improves as additional data become available.

9 Conclusions

AWS Truepower produced a wind-plant output dataset spanning two years at 10-minute time resolution for wind projects in Hawaii. Hourly synthetic wind-plant forecasts for one, four, six, and 24 hours ahead were also produced using a probabilistic method based on actual forecasts. Last, two years of synthetic 2-second and 1-minute plant output data was produced for each site. After extensive validation, it is concluded that the datasets are suitable for use in integration and transmission studies.

10 Acknowledgments

AWS Truepower would like to acknowledge HECO, Hawaiian Electric and Light Company (HELCO), and Maui Electric Company (MECO) for providing meteorological and plant data used in this study.

APPENDIX

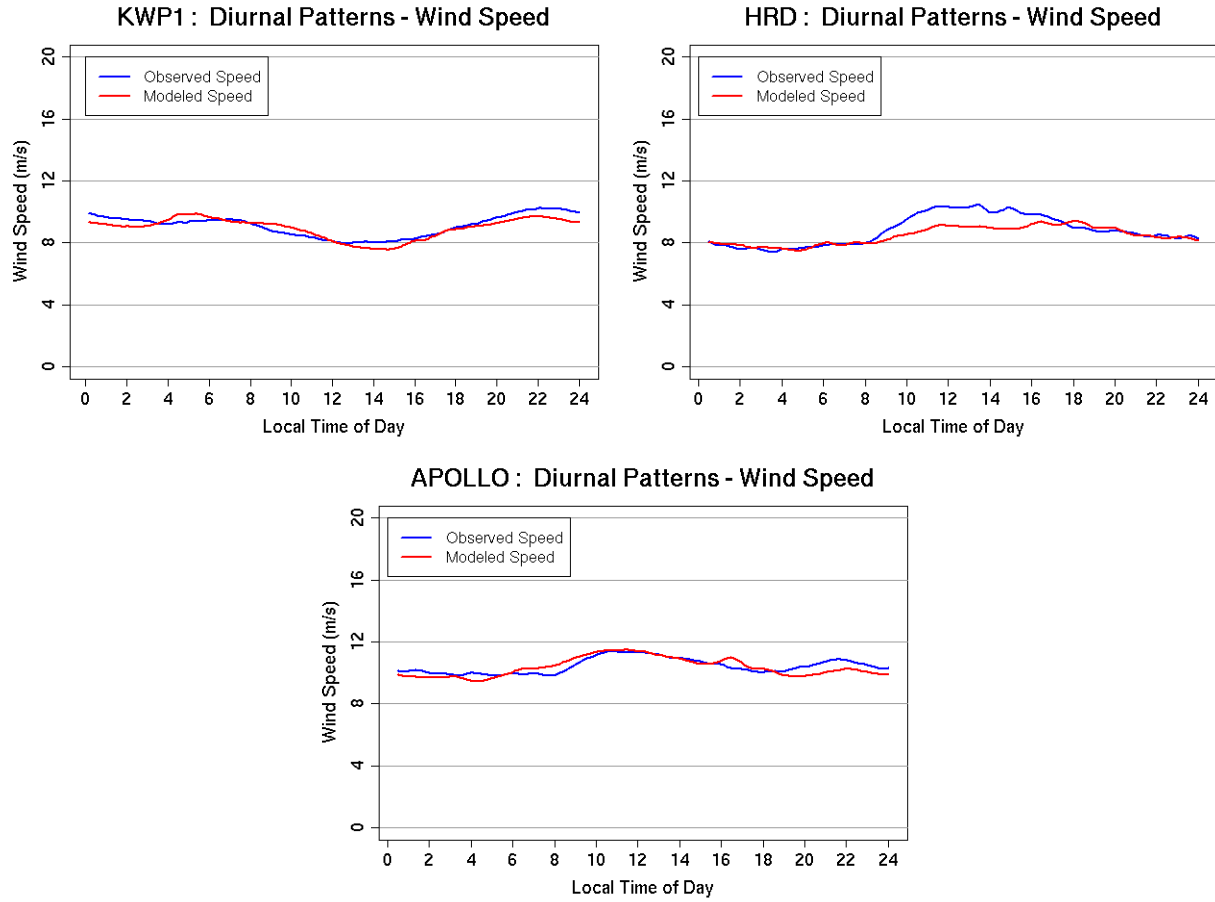


Figure A.1 – Comparison of simulated and observed diurnal mean wind-speeds for three validation projects; KPW1 (top left), HRD (top right), and Apollo (bottom).

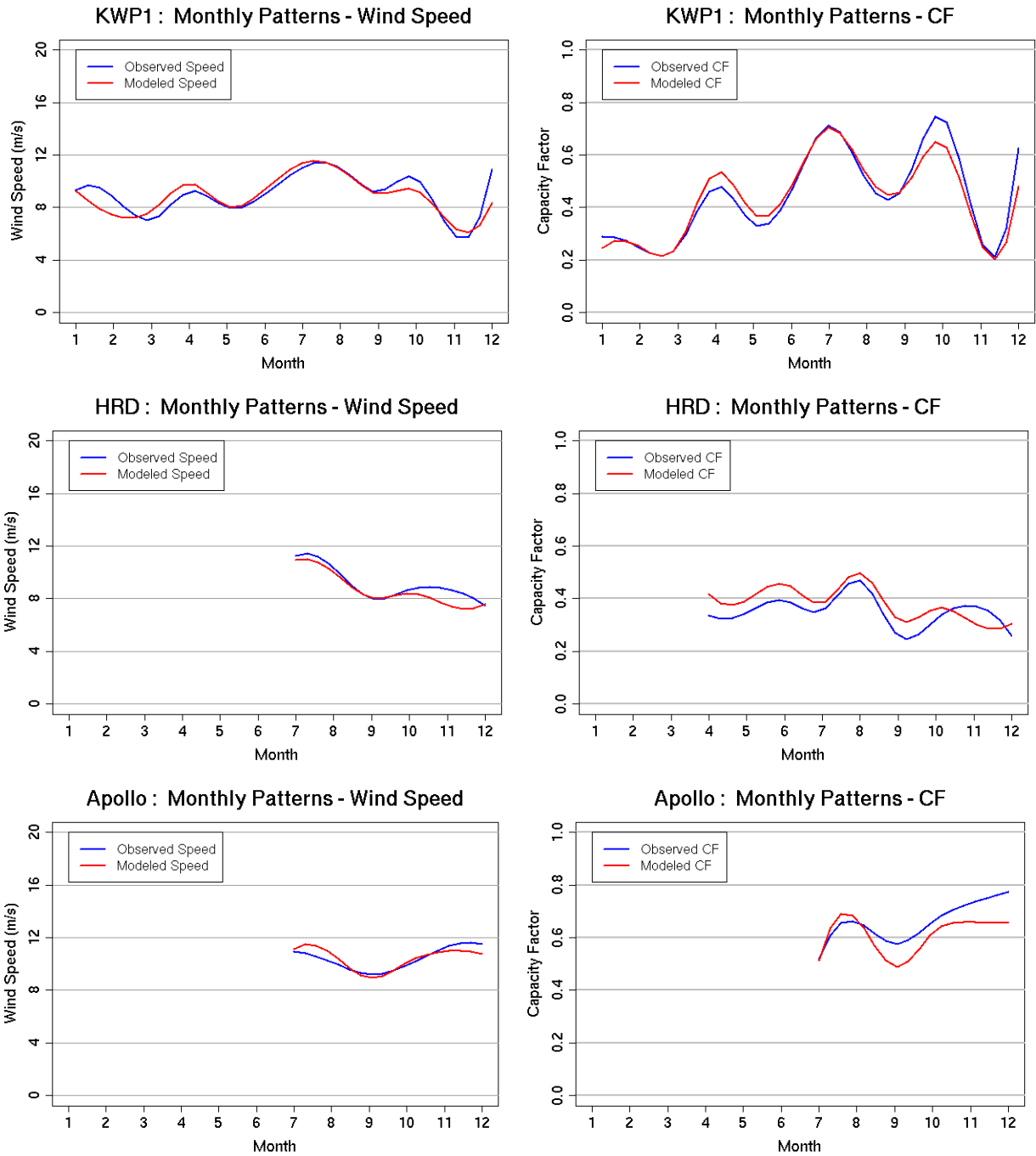


Figure A.2 – Comparison of simulated and observed monthly mean wind speed (left column) and capacity factor (right column) for three validation projects, KPW1 (top), HRD (middle), and Apollo (bottom).

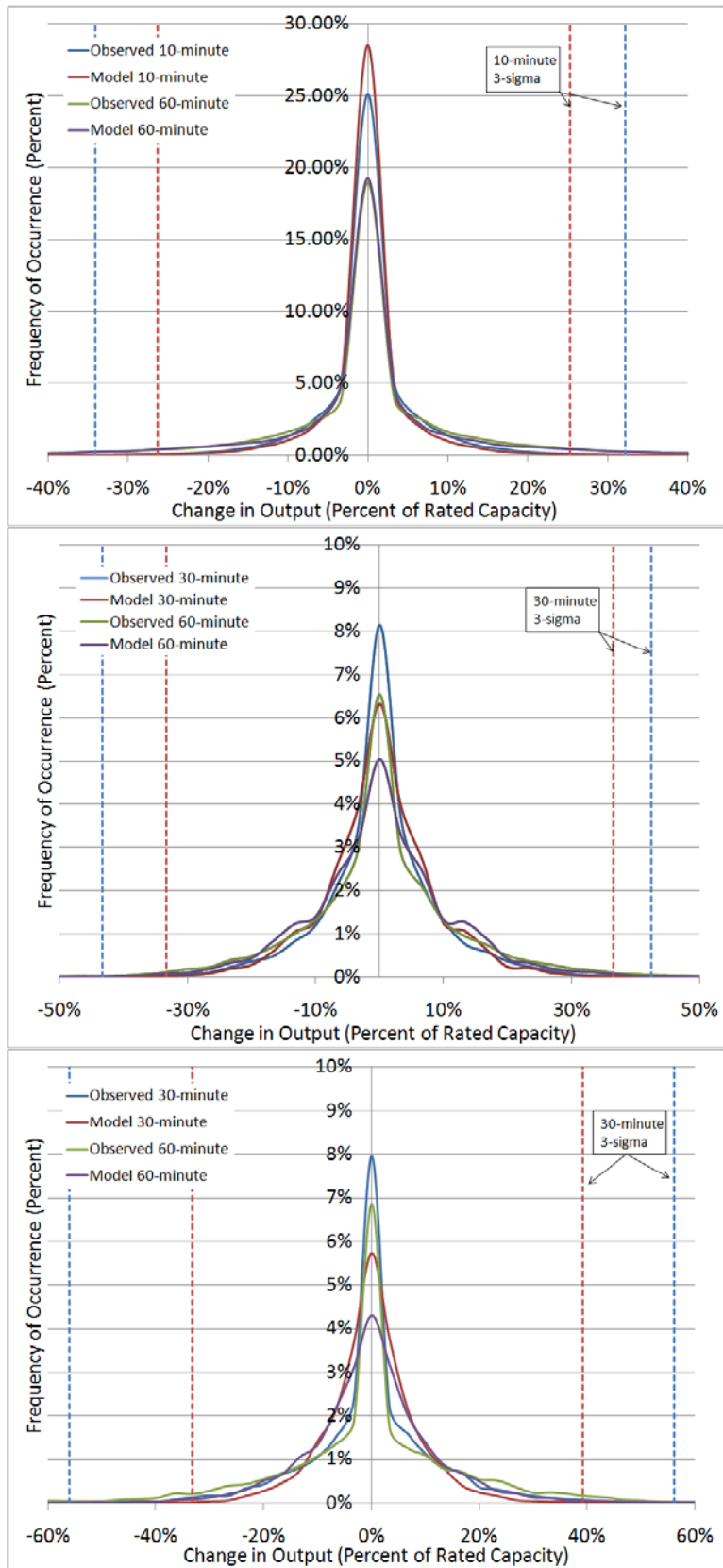


Figure A.3 – Comparison of simulated and observed power ramps for KPW1 (top), HRD (middle), and Apollo (bottom).

Table A.1 – Comparison of observed and modeled power ramps for KPW1 (top), HRD (middle), and Apollo (bottom) for 10-minute and 60-minute time intervals.

KWP1	10-minute		60-minute	
	Observed	Modeled	Observed	Modeled
3-Sigma Down Ramp MW	-10.2	-7.9	-20.4	-20.9
3-Sigma Up Ramp MW	9.7	7.6	20.8	18.6
25% Down Ramp Frequency	228	84	2049	2046
25% Up Ramp Frequency	205	73	2076	1948
40% Down Ramp Frequency	33	10	679	662
40% Up Ramp Frequency	31	10	699	574

HRD	10-minute		60-minute	
	Observed	Modeled	Observed	Modeled
3-Sigma Down Ramp MW	-4.8	-3.7	-5.8	-4.5
3-Sigma Up Ramp MW	4.7	4.0	5.9	5.0
25% Down Ramp Frequency	214	110	502	333
25% Up Ramp Frequency	233	137	659	418
40% Down Ramp Frequency	92	13	213	84
40% Up Ramp Frequency	95	54	334	134

Apollo	10-minute		60-minute	
	Observed	Modeled	Observed	Modeled
3-Sigma Down Ramp MW	-11.8	-7.0	-14.9	-9.2
3-Sigma Up Ramp MW	11.8	8.2	15.0	10.7
25% Down Ramp Frequency	543	99	1229	412
25% Up Ramp Frequency	587	143	1229	495
40% Down Ramp Frequency	183	12	520	65
40% Up Ramp Frequency	176	32	542	143

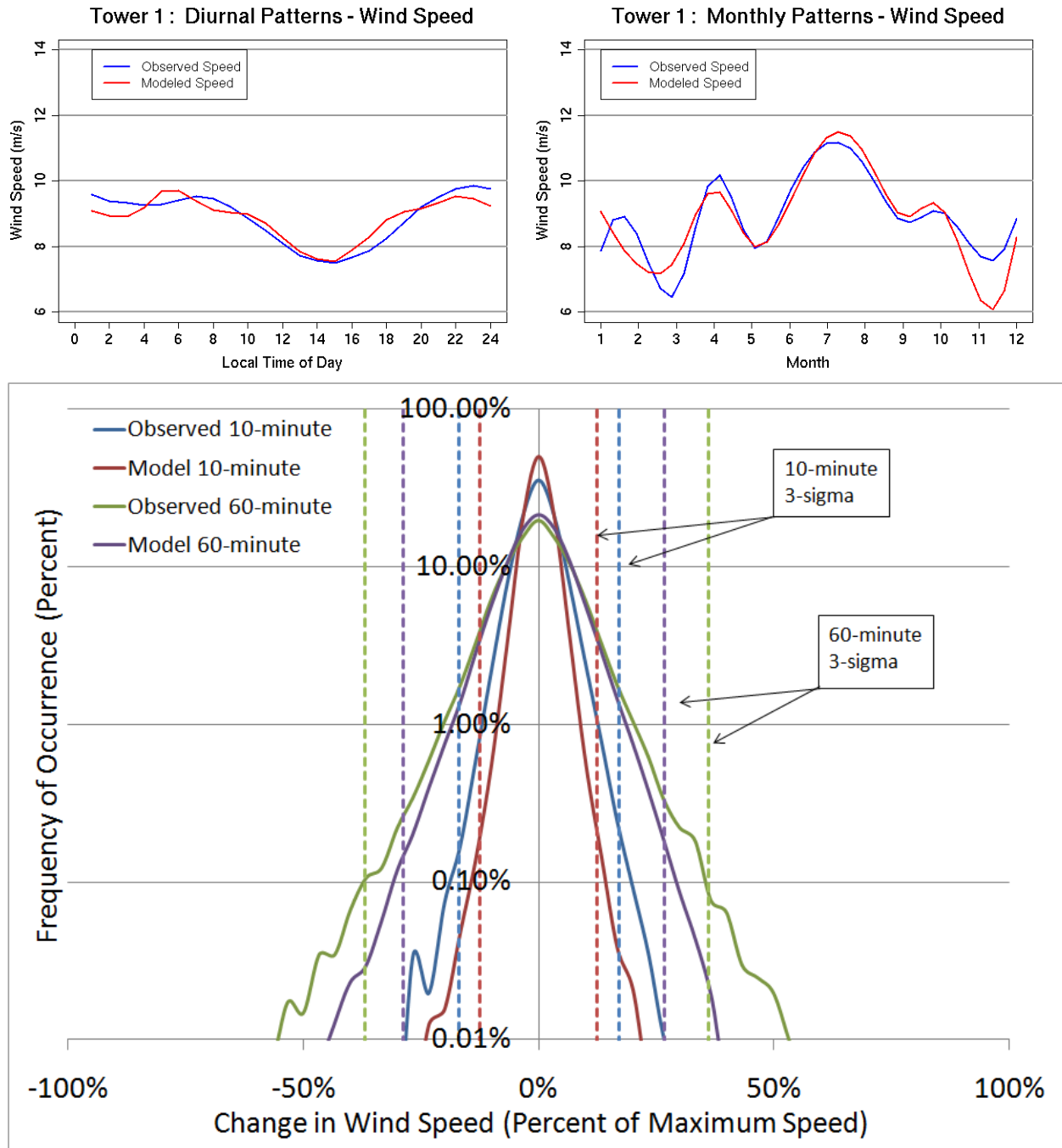


Figure A.4 – Comparison of simulated and observed wind-speed diurnal (top left) and monthly (top right) patterns, as well as 10-minute and 60-minute changes in wind speed (bottom) at Tower 1.

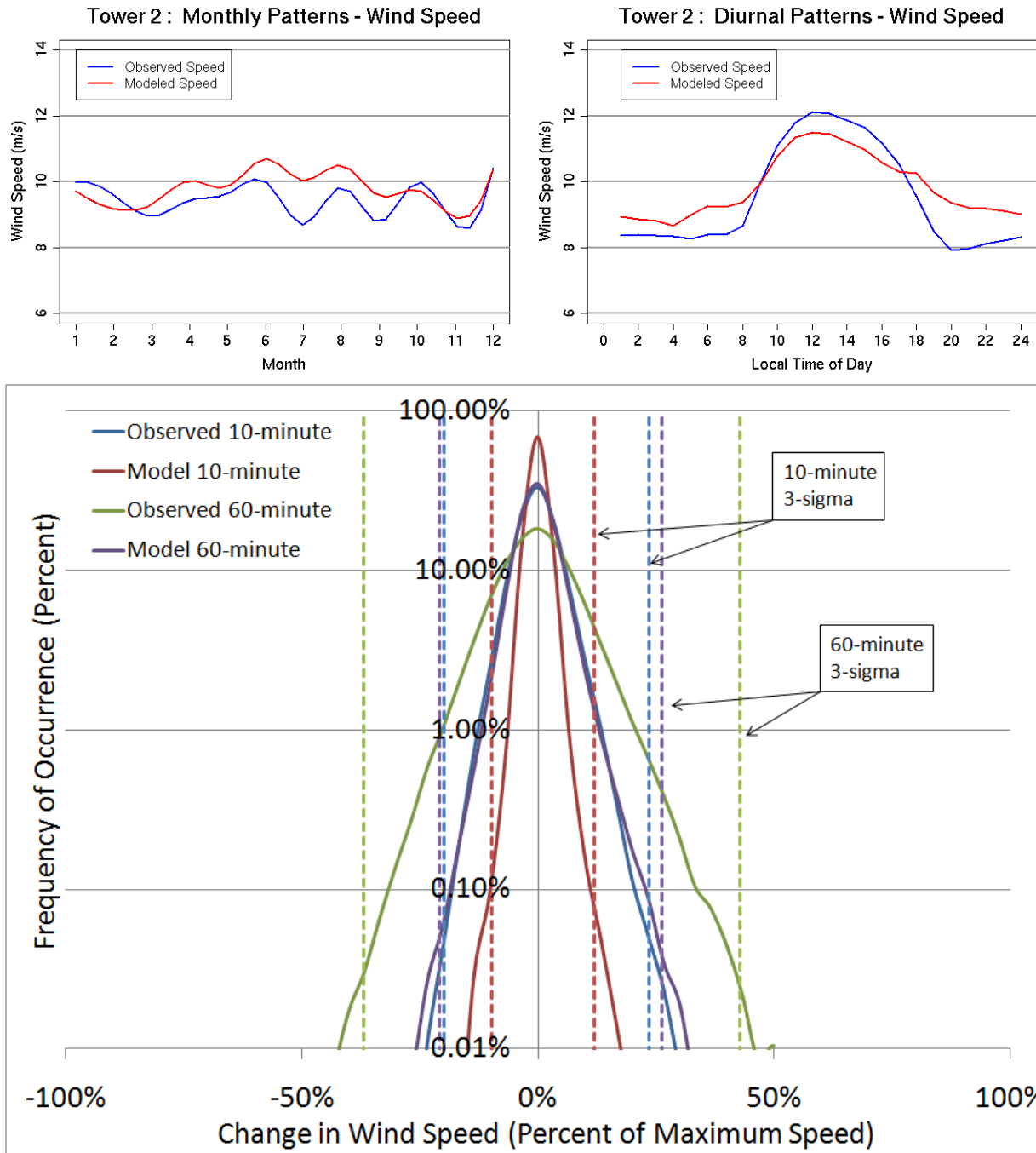


Figure A.5 – Comparison of simulated and observed wind-speed diurnal (top left) and monthly (top right) patterns, as well as 10-minute and 60-minute changes in wind speed (bottom) at Tower 2.

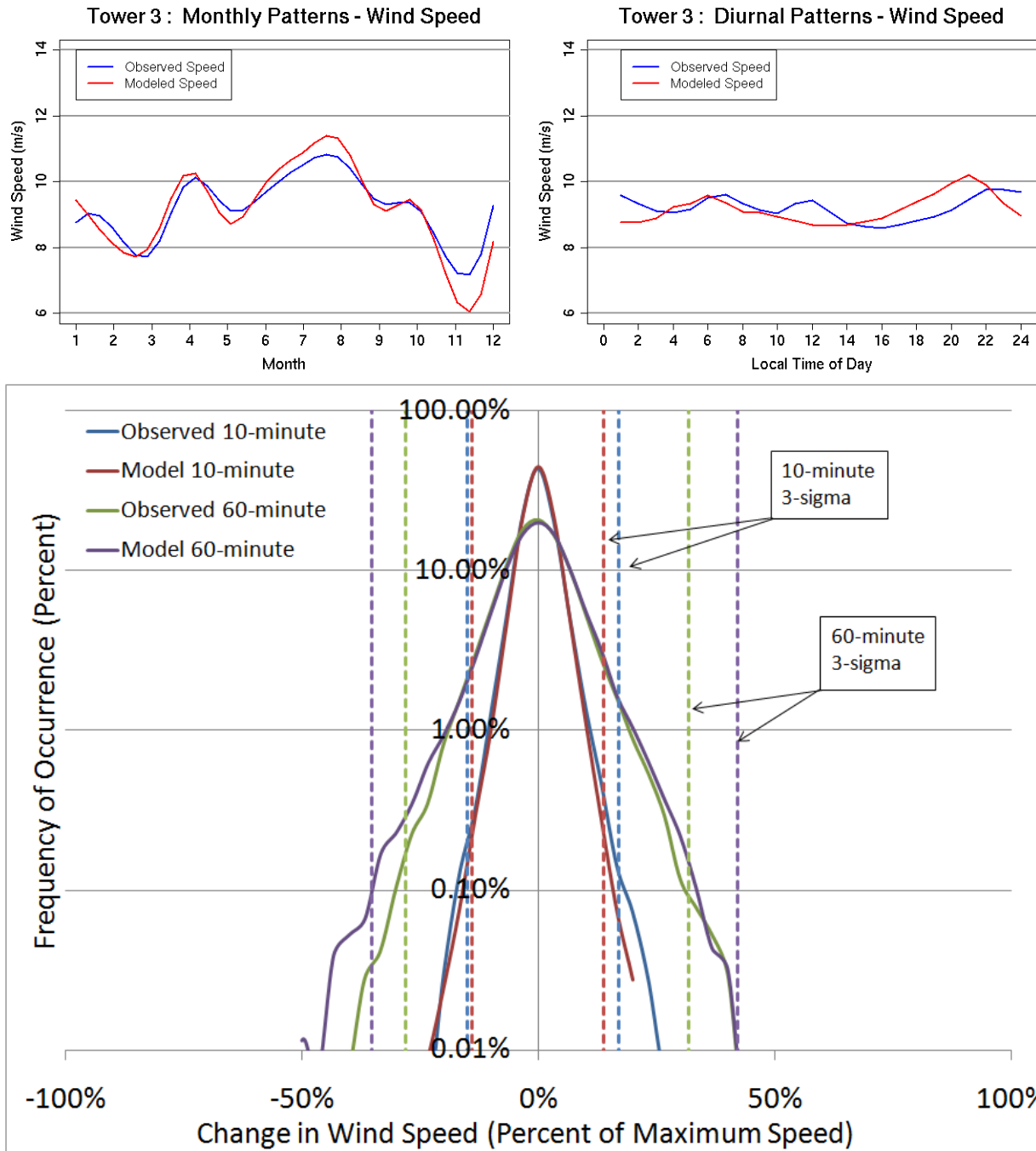


Figure A.6 – Comparison of simulated and observed wind-speed diurnal (top left) and monthly (top right) patterns, as well as 10-minute and 60-minute changes in wind speed (bottom) at Tower 3.

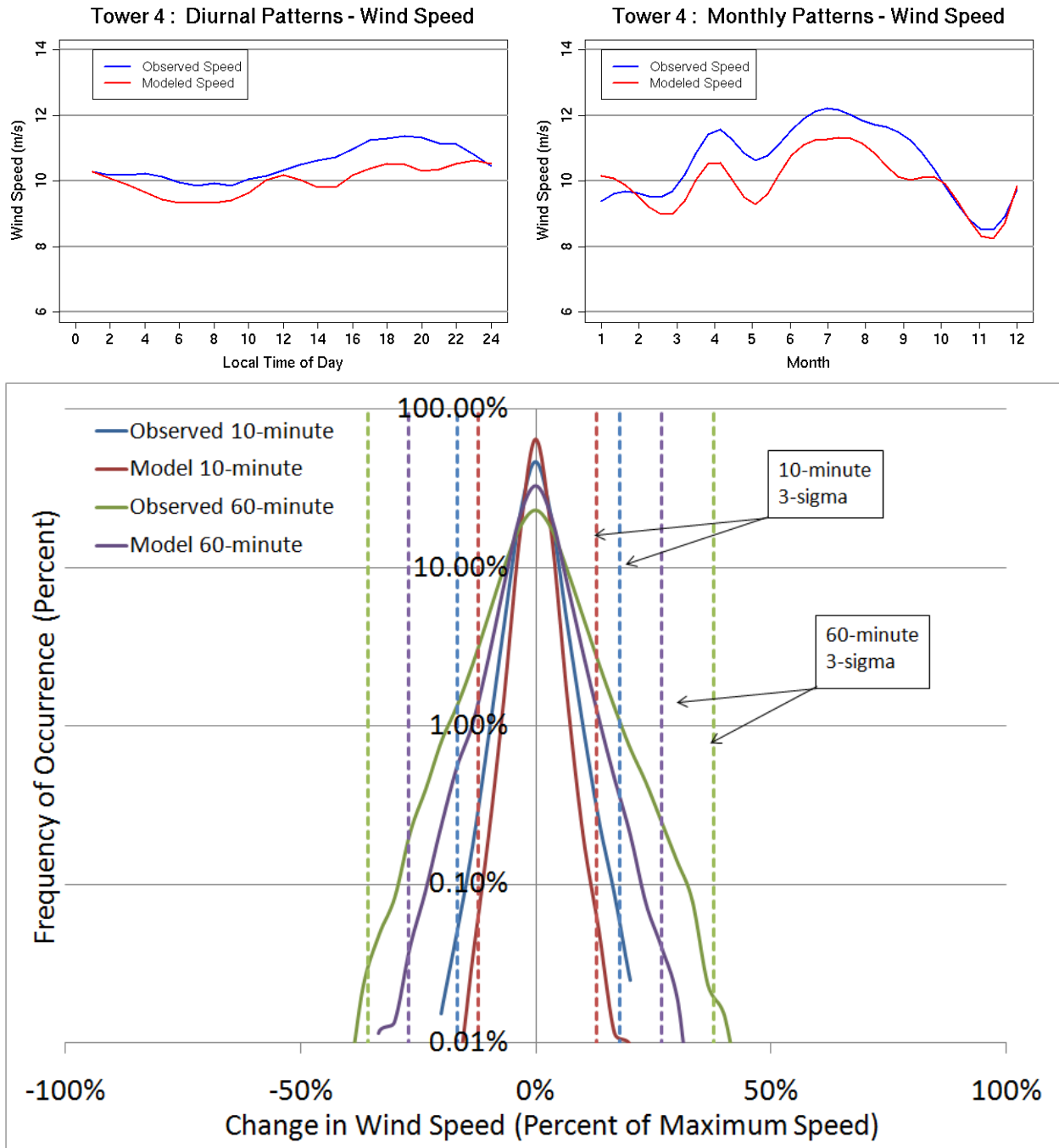


Figure A.7 – Comparison of simulated and observed wind-speed diurnal (top left) and monthly (top right) patterns, as well as 10-minute and 60-minute changes in wind speed (bottom) at Tower 4.

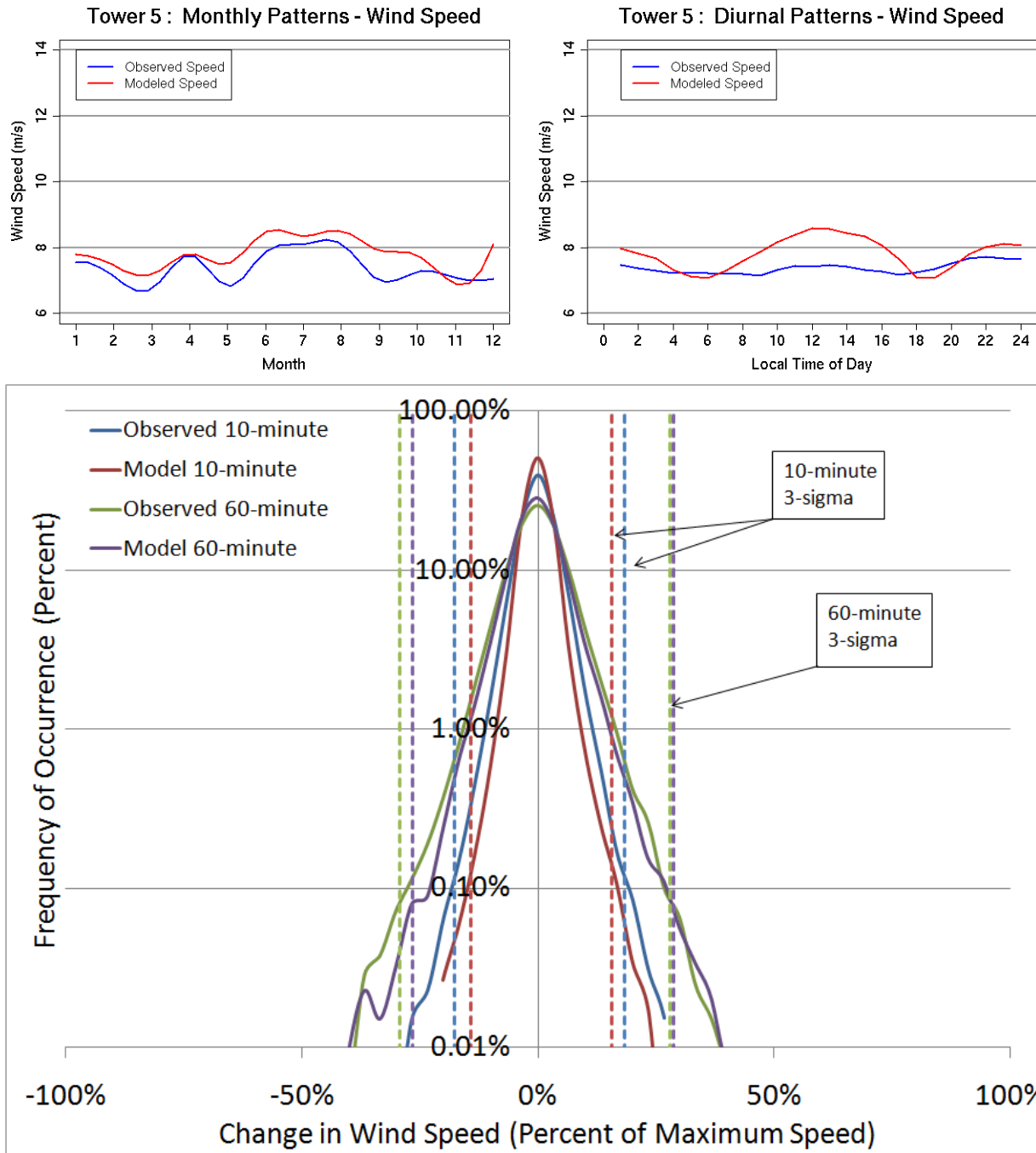


Figure A.8 – Comparison of simulated and observed wind-speed diurnal (top left) and monthly (top right) patterns, as well as 10-minute and 60-minute changes in wind speed (bottom) at Tower 5.

REPORT DOCUMENTATION PAGE

Form Approved
OMB No. 0704-0188

The public reporting burden for this collection of information is estimated to average 1 hour per response, including the time for reviewing instructions, searching existing data sources, gathering and maintaining the data needed, and completing and reviewing the collection of information. Send comments regarding this burden estimate or any other aspect of this collection of information, including suggestions for reducing the burden, to Department of Defense, Executive Services and Communications Directorate (0704-0188). Respondents should be aware that notwithstanding any other provision of law, no person shall be subject to any penalty for failing to comply with a collection of information if it does not display a currently valid OMB control number.

PLEASE DO NOT RETURN YOUR FORM TO THE ABOVE ORGANIZATION.

1. REPORT DATE (DD-MM-YYYY) July 2010		2. REPORT TYPE Subcontract Report		3. DATES COVERED (From - To) 2009 - 2010	
4. TITLE AND SUBTITLE Development of Regional Wind Resource and Wind Plant Output Datasets for the Hawaiian Islands: Final Report			5a. CONTRACT NUMBER DE-AC36-08-GO28308		
			5b. GRANT NUMBER		
			5c. PROGRAM ELEMENT NUMBER		
6. AUTHOR(S) J. Manobianco, C. Alonge, J. Frank, and M. Brower			5d. PROJECT NUMBER NREL/SR-550-48680		
			5e. TASK NUMBER IDHW9174		
			5f. WORK UNIT NUMBER		
7. PERFORMING ORGANIZATION NAME(S) AND ADDRESS(ES) AWS Truepower, LLC 263 New Karner Road Albany, New York 12205				8. PERFORMING ORGANIZATION REPORT NUMBER ACO-8-88500-01	
9. SPONSORING/MONITORING AGENCY NAME(S) AND ADDRESS(ES) National Renewable Energy Laboratory 1617 Cole Blvd. Golden, CO 80401-3393				10. SPONSOR/MONITOR'S ACRONYM(S) NREL	
				11. SPONSORING/MONITORING AGENCY REPORT NUMBER NREL/SR--550-48680	
12. DISTRIBUTION AVAILABILITY STATEMENT National Technical Information Service U.S. Department of Commerce 5285 Port Royal Road Springfield, VA 22161					
13. SUPPLEMENTARY NOTES NREL Technical Monitor: Debra Lew					
14. ABSTRACT (Maximum 200 Words) In March 2009, AWS Truepower was engaged by the National Renewable Energy Laboratory (NREL) to develop a set of wind resource and plant output data for the Hawaiian Islands. The objective of this project was to expand the methods and techniques employed in the Eastern Wind Integration and Transmission Study (EWITS) to include the state of Hawaii.					
15. SUBJECT TERMS Hawaii; wind integration; resource data; EWITS; OWITS; power; grid					
16. SECURITY CLASSIFICATION OF:			17. LIMITATION OF ABSTRACT UL	18. NUMBER OF PAGES	19a. NAME OF RESPONSIBLE PERSON
a. REPORT Unclassified	b. ABSTRACT Unclassified	c. THIS PAGE Unclassified			19b. TELEPHONE NUMBER (Include area code)

Standard Form 298 (Rev. 8/98)
Prescribed by ANSI Std. Z39.18